Full scale low-cost ultra wide band antenna for SKA low frequency array

by

Dewald Hermanus Schoeman

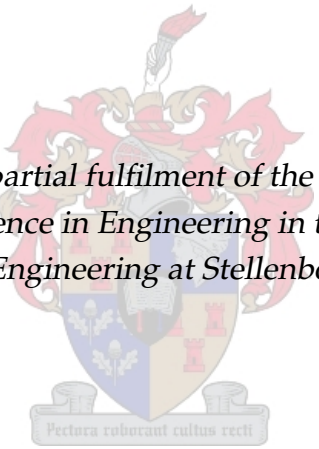

Thesis presented in partial fulfilment of the requirements for the degree of Master of Science in Engineering in the Faculty of Electrical and Electronic Engineering at Stellenbosch University

Supervisor: Dr. D.I.L. de Villiers

March 2013

Declaration

By submitting this thesis electronically, I declare that the entirety of the work contained therein is my own, original work, that I am the sole author thereof (save to the extent explicitly otherwise stated), that reproduction and publication thereof by Stellenbosch University will not infringe any third party rights and that I have not previously in its entirety or in part submitted it for obtaining any qualification.

March 2013

Abstract

Full scale low-cost ultra wide band antenna for SKA low frequency array

D.H. Schoeman

Department of Electrical and Electronic Engineering,
University of Stellenbosch,
Private Bag X1, 7602 Matieland, South Africa.

Thesis: MScEng (E&E)

March 2013

This thesis is about the design, simulation and measuring of ultra wide band antennas for use in the Square Kilometre Array (SKA).

The SKA is a radio astronomy project with one of the aims of detecting hydrogen particles in deep space. Several thousand antennas over a wide band of frequencies are needed to receive the radiation from these particles. This motivates the need for a low-cost ultra wide band antenna with the focus on the low frequency part of the SKA.

In this thesis we present two design strategies:

The first design strategy is for a printed LPDA on a substrate and design curves are generated. A scale model was built and measurements did not correlate with simulation results. This is due to manufacturing tolerances and assembly of the pyramidal structure.

The second design strategy is for a full scale zig-zag antenna and design curves were also generated. The aim here is to produce a low-cost prototype by using brazing rods for the wire structure and mount it on a wooden frame. A full scale model was built and measurements on the roof produced much interference for the radiation pattern, but the reflection coefficient was good. We suggest doing measurements in an interference free environment in order to achieve the needed results.

To conclude we suggest using the zig-zag antenna for the SKA. Some issues do however need more attention as the transformer has some losses, the cross polarisation is probably not good enough and the beamwidth does not reach the specification. We demonstrated a low cost prototype and there is the possibility of low-cost large scale manufacturing but

this needs to be addressed. This has however not been analysed as many factors for large scale manufacturing are very difficult to predict beforehand and lies outside the scope of this thesis.

[302 words]

Opsomming

Volskaal lae-koste ultrawyeband antenna vir SKA lae-frekwensie opstelling

("Full scale low-cost ultra wide band antenna for SKA low frequency array")

D.H. Schoeman

Departement Elektriese en Elektroniese Ingenieurswese,
Universiteit van Stellenbosch,
Privaatsak X1, 7602 Matieland, Suid Afrika.

Tesis: MScIng (E&E)

Maart 2013

Hierdie tesis gaan oor die ontwerp, simulasie en opmeting van ultrawyebandantennas vir gebruik in die SKA ("Square Kilometre Array").

Die SKA is 'n radioastronomie projek met die doel om waterstof partikels op te spoor in die ruimte. Duisende antennas wat oor 'n wye band van frekwensies strek is nodig om die energie van die partikels op te vang. Hieruit is daar 'n aanvraag vir lae-koste ultrawyebandantennas met die fokus op die lae frekwensie deel van die SKA.

In hierdie tesis word twee ontwerpstrategieë voorgestel:

Die eerste ontwerpstrategie is vir 'n gedrukte logaritmies periodiese dipool reeks (LPDR) op 'n substraat tesame met ontwerpskurwes wat gegenereer word. 'n Skaal model is gebou en die gemete resultate stem nie ooreen met die simulasie nie. Dit kan toegeskryf word aan vervaardigingstoleransies en die aanmekaar sit van die piramide struktuur.

Die tweede ontwerpstrategie is vir 'n vol skaal sigsag ("zig-zag") antenna met ontwerpskurwes wat ook gegenereer word. Die doel is om 'n lae-koste prototipe te bou deur sweissoldeerdraad te gebruik vir die draadstruktuur en dan op 'n hout raam te plaas. 'n Vol skaal model is gebou en metings op die dak het baie interferensie veroorsaak vir die stralingsveld, maar tog was die weerkaatskoëffisient goed. Ons stel voor om die metings te herhaal in 'n steuringvrye omgewing om sodoende die korrekte resultate te verkry.

Om af te sluit stel ons voor om die sigsag antenna vir die SKA te gebruik. Sekere kwessies soos die transformator wat verlieserig is, die kruispolarisasie wat moontlik nie goed

genoeg is nie en die bundelwydte wat nie die spesifikasie haal nie moet nog aandag geniet. Ons het 'n lae-koste prototipe gedemonstreer en daar is die moontlikheid om dit op grootskaalse vervaardiging ook goedkoop te doen, maar dit moet nog uigesorteer word. Dit was wel nie geanaliseer nie, siende dat vele faktore 'n rol speel by grootskaalse vervaardiging wat uiters moeilik is om voor die tyd te voorspel en buite die omvang van die tesis lê.

[324 woorde]

Acknowledgements

I would like to express my thanks to the following institutions and individuals:

- Electronic Engineering Department of Stellenbosch University for providing the necessary facilities to complete my degree.
- Dr. Dirk de Villiers for his leadership and vast amount of knowledge.
- Prof. Keith Palmer for his endless experience and ideas.
- Mr. Wessel Croukamp for his part in building various parts for the antenna's.

Dedications

To all my friends at university, may you all succeed in life.

Contents

List of Figures

List of Tables

Nomenclature

Abbreviation	Description	Definition
SKA	Square Kilometre Array	page 1
f	Frequency	General
c	Speed of light in free space ($\approx 2.998 \times 10^8$ m/s)	General
v	Speed of a wave in a medium	General
λ	Wavelength	General
mc/s	Megacycles per second (replaced by Hertz)	General
MHz	Mega Hertz	General
GHz	Giga Hertz	General
l	Distance between 2 objects or elements	General
Ω	Ohm	General
E-field	Electric field	General
H-field	Magnetic field	General
$\vec{x}$	Vector notation	General
ϵ_0	Permittivity of free space ($\approx 8.854 \times 10^{-12}$ F/m)	General
ϵ_r	Permittivity of a dielectric material (dimensionless)	General
μ_0	Permeability of free space ($4\pi \times 10^{-7}$ H/m)	General
μ_r	Permeability of a dielectric material (dimensionless)	General
ρ	Rho	General
J	Current Density	General
∇	Del	General
r	Radial distance	General
θ	Theta angle	General
ϕ	Phi angle	General
U	Radiation Intensity	General
k	Phase constant	General
η	Intrinsic impedance	General
W	Power density	General
P	Radiated power	General
D	Directivity	General
R_r	Radiation resistance	General
Z_w	Wave impedance	General
R_n	Distance of the n'th dipole	General
f_n	The n'th frequency	General
l_n	Length of the n'th dipole	General

Abbreviation	Description	Definition
s_n	Center gap at the n'th dipole	General
d_n	Diameter of the n'th dipole	General
B_s	Designed band width	page 21
B	Chosen band width	page 21
B_{ar}	Active region of the band width	page 21
L	Total length of the structure	page 21
l_{max}	Length of the longest dipole	page 21
λ_{max}	Largest wavelength	page 21
N	Number of elements	page 21
Z_a	Average characteristic impedance of the element	page 21
S_{11}	Reflection coefficient	page 38
$^\circ$	Degrees	General
R_{in}	Input impedance (Real)	page 22
Z_{in}	Input impedance	page 38
F_a	Roundness factor	page 33
CP	Cross Polarisation	page 39
α	Apex half angle	page 4
γ	Apex angle	page 34
F/B	Front-to-back ratio	page 34
τ	Geometric ratio	page 4
PCB	Printed Circuit Board	page 50
F	Function	page 11
K	Constant parameter	page 11
MoM	Method of Moments	page 28
LNA	Low-noise amplifier	page 63

Chapter 1

Introduction

This thesis aims to provide a design strategy for an antenna as an option for the low frequency array of the Square Kilometre Array (SKA) [6] and SKA South Africa [7].

1.1 Motivation for this work

This thesis aims to develop a design strategy for an ultra wide band antenna as an option for the SKA project.

The SKA will be built in South Africa and Australia and is likely to consist of 3 types of receiving antennas [6]:

- Dishes (0.45-10 GHz)
- Mid frequency aperture array stations (0.4-1.4 GHz)
- Low frequency array stations (0.07-0.45 GHz)

with the first two assigned to South Africa and the third to Australia.

Hydrogen (H_1) is abundant in space and is part of the raw material from which stars are formed. Hydrogen atoms radiate at 1.42 GHz (wavelength of 21 cm), which results from the movement between two energy levels related to the spin vector of the electron [8]. The hydrogen proton and electron spin in the same direction, but can randomly change spin direction emitting energy that a radio telescope can detect. Change in spin direction occurs rarely for hydrogen atoms, but is frequently detected due to the large quantities in space. These atoms experience redshift (similar to the Doppler effect) and wide band antennas are required to detect a range of atoms at various distances at the same time. The low frequency array is needed to detect very far away hydrogen.

South Africa is currently building the MeerKAT telescope as a precursor to the SKA while Australia is building ASKAP (Australian SKA Pathfinder) as the precursor for Australia [6].

1.1.1 Project timeline and Location

The SKA was conceptualised in 1991 and a short listing of suitable sites was made in 2006. 2008-2012 showed conceptual telescope designs with the site selection made in 2012. 2013-2015 will have a detailed design and pre-construction phase with phase one construction planned for 2016-2020. The full operation of phase one is scheduled for 2020 with phase two also starting and full operation planned for 2024.

The SKA will be built in the Karoo in South Africa and in Western Australia. These sites were found favourable for this project according to the following selection criteria: [6]

- Radio frequency interference from electrical devices
- Characteristics of the ionosphere and troposphere
- Physical characteristics including climate
- Connectivity for the telescope self and to networks for worldwide distribution of data
- Infrastructure costs (power supply and distribution)
- Maintenance and operational costs
- Long term sustainability of site as a radio quiet zone

1.2 About this project

We will design and test a prototype antenna for the SKA low frequency array. The antenna must be able to be mass produced for use in the SKA, as several thousand ($\approx$500,000) are likely to be required.

We put some constraints on the prototype that we aim to build. It should operate in the frequency band of 70 to 450 MHz and should not be too big. This is quite a loosely defined term and thus we limit the physical size to a $1m^2$ (1m $\times$ 1m) footprint for this antenna. A half-wavelength dipole with a length of 1m is resonant at 150 MHz and this suggest the limit for the lower frequency of the antenna. The upper frequency can easily be increased to 500 MHz.

For the SKA we want to build many antennas, thus it also needs to be inexpensive to fit in the budget. The budget for the whole project is likely to be R20 billion (€1,500 million) [7] and this thesis aims to minimise the costs for this part of the project. We use a wire antenna as this excludes expensive dielectrics and possible machinery that goes with it.

We are uncertain of the exact LNA (Low-noise amplifier) design and configuration for the feed and this places the focus on the radiation pattern.

In this thesis we aim to develop a design strategy for a prototype antenna. This design aids in designing and building an antenna that fulfils a certain specification.

Other researchers [9] [10] [11] are also working on antennas for the SKA project. We will compare our results with their results and discuss the different aspects in terms of performance and costs.

We first look at the characteristics of a single dipole and soon realise that this is not sufficient. We then look at dipole arrays and see much broader bandwidths and more directed radiation patterns. By placing these dipoles certain distances apart and using different lengths we can achieve a multitude of different bandwidths and radiation patterns. One possibility is to make the dipoles and spacings logarithmically longer and also the spaces between them as proposed by DuHamel and Isbell [12], [13].

This method consists of designing the antenna such that the characteristics are periodic with the logarithm of the frequency. If the variation of the characteristics over a single period are small it results in a broadband antenna. Bandwidths of 10:1 have been obtained with this method and even greater bandwidths are possible [12].

Before 1960 log-periodic antennas have all consisted out of a single element which is shaped to provide the log-periodic characteristics. The antennas introduced by Isbell [13] show that the log-periodic principles can be extended to the design of arrays that consists of conventional elements.

Next we look at Carrel's work [2] and follow his design strategy. By only using his strategy we get an antenna which fulfils a certain specification, but still lack the requirements for the SKA (such as dual polarisation and beamwidth). We now extend his work to 3 dimensions as shown by Dubrovka et al. [4] by using another identical antenna to improve the radiation pattern. The second antenna is a mirror image of the first one and the two are separated by an angle. For dual polarisation we rotate the two antennas by 90° around their axis. Figure 3.25 shows a manufactured LPDA model for this dual polarised design.

We perform a parameter study on the 3 primary parameters according to Carrel's [2] design. We simulate and build a 4 arm, dual polarised log-periodic dipole array (LPDA) antenna. This we do on FR4 printed circuit board. The operating frequency is 1.5 GHz to 6 GHz for a scale model. We choose this frequency band as it simplifies the measurements for the anechoic chamber we use. The chamber works well from around 2 GHz and higher. The high frequency limit is mainly due to manufacturing tolerances.

Simulation is done in FEKO by scripting in EDITFEKO. MATLAB processes the data and the informations is shown. A prototype is built and measured in the anechoic chamber

and the results are compared with the simulated results. A good correlation between the simulated and measured results is observed.

Next we look at the zig-zag antenna configuration as a prototype for the SKA low frequency array. Here the emphasis leans more to low-cost for the prototype.

This concludes the project and we can make a recommendation about the findings in this project.

In this thesis we propose a design strategy for two antennas, namely the LPDA and the zig-zag configuration. This design strategy incorporates Carrel's [2] design strategy for one antenna and DuHamel's [14] for a two antenna configurations. Dual polarisation is achieved by merely rotating the structure as shown by Dubrovka [4]. We optimise the design strategy and build a scale model LPDA on a substrate and a full scale zig-zag prototype and measure them.

By analysing the results we see that the apex half angle (α) dominates the characteristics and the geometric ratio (τ) has little influence. This means that when we change τ, only small differences are observed when compared to α. The parameter τ does however need to be within a certain range to produce ultra wide band characteristics.

1.3 About this thesis

Chapter 2 is the literature study. A design strategy for a log-periodic dipole array antenna was developed by Carrell [2]. This design is extended to a non-planar antenna as suggested by Dubrovka et al. [4].

We start by looking at a single dipole and see if this can fulfil our objectives. This is probably the most simple and inexpensive option we can use. By further investigations we observe that the bandwidth is too small for our application and the radiation pattern is unwanted. We use an LPDA which consists out of using several dipoles at different operating frequencies, thus different lengths, in order to achieve a larger bandwidth. Furthermore we can place these dipoles at certain distances away from each other to change the radiation pattern. We start by using one LPDA, but use more for control over the radiation pattern and dual polarisation.

Chapter 3 is the Dual LPDA. Here we analyse a dual polarised LPDA antenna. We build a scale model on a dielectric board in order to see what characteristics are possible.

Chapter 4 is the Zig-Zag antenna. The main focus is to minimise the costs for a prototype, thus we remove the dielectric. We analyse the Zig-zag configuration and compare it to the Dual LPDA. We build a low-cost prototype and compare the measured results with

the simulation results.

Chapter 5 is the Recommendations and Conclusion. Here we recommend using the zig-zag configuration for the SKA low frequency array. Measured results were unfavourable mostly due to environmental interferences, but better measurements are expected at a much better measurement site. When several thousand antennas need to be manufactured it is almost impossible to say beforehand which design would be most cost effective. In this thesis we aim to keep material costs down for the antenna. For the SKA however there still needs to be looked at other contributing cost factors such as assembly lines needed, labour, testing products, roll out, maintenance and replacement.

The contributions made in this thesis are as follow:

- Design strategy for a printed LPDA antenna.
- Design strategy for a full scale zig-zag antenna.
- Building and testing (through measurement) these two antennas.

1.4 Recap

In this chapter the following was discussed:

1. the need for ultra wide band antennas for SKA purposes
2. the SKA project
3. this thesis as part of the SKA project

Chapter 2

Literature study

A simple and inexpensive antenna is the wire antenna. We first look at an infinitesimal wire antenna when the length (l) is much shorter than the wavelength (λ). This wire produces a doughnut-shaped radiation pattern with a very small radiation resistance which needs improvement. One way to improve this is to make use of an array of dipoles that "work together" to shape the radiation pattern in the form that is needed for this thesis.

The input impedance is also of concern, but is very low (for $l = \lambda/50$ the radiation resistance is $R_r < 1\ \Omega$) for the infinitesimal antenna and can be increased by increasing the length. A commonly used antenna is the half-wavelength ($l = \lambda/2$) dipole which has a radiation resistance of 73 Ω. This is very close to the 75 Ω characteristic impedance of some transmission lines and produces very small reflections according to Balanis [1].

2.1 Infinitesimal Dipole

The main characteristic properties of this dipole will now follow with the electric field and the radiated power in the far-field and the radiation resistance. For this dipole we approximate the current on the wire to be constant as the length is much shorter than the wavelength. The far-field region is where the distance between the sender and receiver (R_{sr}) is at least

$$R_{sr} \geq \frac{2D_{sr}^2}{\lambda} \tag{2.1}$$

with D_{sr} being the largest dimension of the antenna and λ the wavelength [1].

In this region the electric field has only a θ-component which is

$$E_\theta = j\eta \frac{kI_0 l e^{-jkr}}{4\pi r} \sin\theta \tag{2.2}$$

and a magnetic field component of

$$H_\phi = j\frac{kI_0 l e^{-jkr}}{4\pi r} \sin\theta \tag{2.3}$$

with η being the intrinsic impedance, $k = \omega\sqrt{\mu\epsilon}$ being the wave number, I_0 the current on the dipole, l the length of the dipole and r the distance from the dipole. The power density is

$$W_r = \frac{\eta}{2}\left(\frac{kI_0 l}{4\pi r}\right)^2 \sin^2\theta \tag{2.4}$$

which leads to the radiation resistance which is found by equating the radiated power to the power absorbed by the antenna in the circuit.

$$P_{rad} = \frac{\eta}{12\pi}k^2 I_0^2 l^2 = \frac{1}{2}|I_0|^2 R_r \tag{2.5}$$

Where R_r is the radiation resistance, which simplifies to

$$R_r = 80\pi^2\left(\frac{l}{\lambda}\right)^2 \tag{2.6}$$

for a free-space medium ($\eta \approx 120\pi$) and $k = 2\pi/\lambda$. For a wire to fall in this classification it must be very short ($l \leq \lambda/50$).

As an example we calculate the radiation resistance of this short dipole that is $l = \lambda/50$. At a frequency of 300 MHz the wavelength is $\lambda = c_0/f$ which is 1 m which results in $l = 20$ mm. By using (2.6) above this leads to $R_r = 0.316\ \Omega$. We would like to connect an available transmission line (available ones are mostly 50 Ω cables in our lab) directly to this dipole, but due to the large difference in impedance between these two it results in a large mismatch meaning most of the power gets reflected.

This concludes a brief description of the infinitesimal dipole. The radiation pattern and resistance is of great importance but unfortunately the resistance is quite low. The resistance is dependent on the length of the dipole, thus by increasing the length should also increase the resistance. Now we increase the dipole length in order to have a favourable resistance.

2.2 Half-wavelength Dipole

For an antenna to have a favourable resistance, we want it to be very close to the characteristic impedance of the transmission line. This will ensure very small reflections and improve efficiency. The half-wavelength dipole is resonant at about 73 Ω and thus 75 Ω transmission lines are made [1].

Here we approximate the current on the wire to be sinusoidal as the wire length is comparable to the wavelength. The current is a maximum at the feed point in the centre of the wire and a minimum at the ends of the wire. The power density of the half-wavelength dipole is given by

$$W_r = \eta\frac{|I_0|^2}{8\pi^2 r^2}\frac{\cos^2\left(\frac{\pi}{2}\cos\theta\right)}{\sin\theta} \approx \eta\frac{|I_0|^2}{8\pi^2 r^2}\sin^3\theta \tag{2.7}$$

which when normalised resembles the normalised power density of the infinitesimal dipole closely and the radiated power is

$$P_{rad} = \eta \frac{|I_0|^2}{4\pi} \int_0^{\pi} \frac{\cos^2\left(\frac{\pi}{2}\cos\theta\right)}{\sin\theta} d\theta \approx \eta |I_0|^2 \frac{1.219}{4\pi} \tag{2.8}$$

The integral was evaluated using numerical integration and found to have a value of 1.21883 and subsequently approximated to 1.219.

Now we move onto the bandwidth of this type of antenna. We calculate the bandwidth of this dipole by simulating it in FEKO. Figure 2.1 shows the results of this simulation where the centre frequency of the dipole is 1 GHz and the wire has a diameter of 2 and 6 mm.

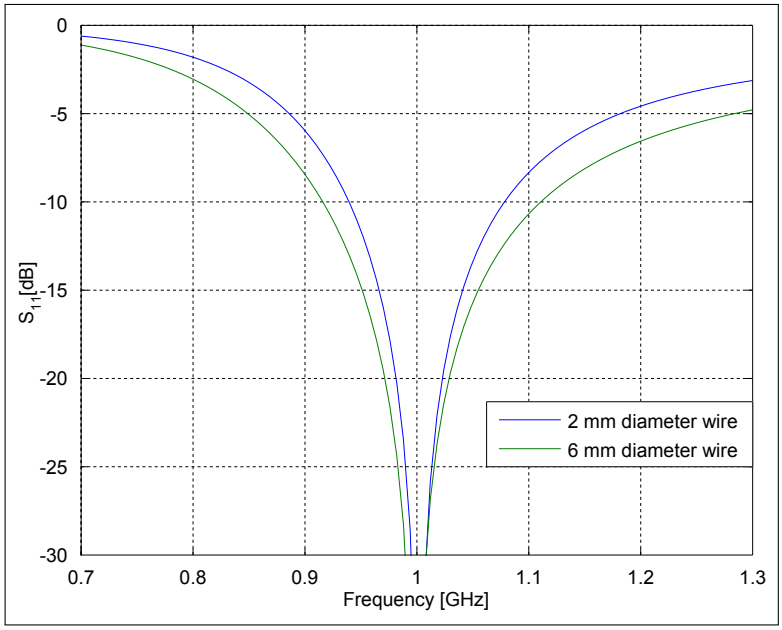

Figure 2.1: S_{11} comparison for a half-wavelength dipole of 2 and 6 mm in diameter.

Here we observe that it is resonant at the centre frequency with a characteristic impedance of 73 Ω. The -10 dB points for the lower and upper frequencies of the 2 mm wire are 0.94 GHz and 1.08 GHz respectively and this results in a bandwidth of 14% for this type of antenna. The 6 mm wire on the other hand results in lower and upper frequencies of 0.92 GHz and 1.11 GHz with a bandwidth of 19%. This shows that the bandwidth can be widened by using a thicker dipole (within certain limits), but this is not very effective as a much thicker wire is needed, which increases the weight and material costs while the bandwidth only increases by 5%. This should serve as reason to not thicken dipoles when large bandwidths are required, but rather look at another possibility. The wire diameter must remain much smaller than the wire length, and if the diameter becomes comparable to the length the antenna characteristics will change.

The parameters that we focussed on mostly, namely the input impedance and the radiation pattern, have been determined for the half-wavelength dipole. Two problems present are the narrow bandwidth of this antenna (14% for a 2 mm wire diameter) and the radiation pattern that is not directed. These problems can however be solved by implementing multiple dipoles to form arrays.

2.3 Dipole Arrays

By using dipole arrays we can solve these two problems at the same time. Dipole arrays can alter the radiation pattern to be more directive in some cases [15]. They can also broaden the bandwidth of the antenna to much more than a single dipole can according to Balanis [1].

2.3.1 Radiation Pattern altering using Arrays

Placing dipoles near each other will affect the radiation pattern of the combined antenna. Arrays consists of similar antennas pointing in the same direction. Certain arrangements of these antennas can produce radiation patterns that are in phase at specific points in space and 180° out of phase at other points. This gives us the ability to alter the radiation pattern and design antennas that radiate in particular directions with very little radiation in other directions [15].

We can design such a radiation pattern because we can control the (1) number of elements, (2) separation between each element and (3) the magnitude and phase feeding each element.

To provide directive patterns it is necessary that the fields from the elements interfere constructively in the desired directions and destructively in the rest. To shape this antenna pattern there are 5 controls according to [1] that can be used and they are:

1. the geometrical configuration of the array
2. the relative displacement between the elements
3. the excitation amplitude of the individual elements
4. the excitation phase of the individual elements
5. the relative pattern of the individual elements

The simplest way of forming an array is by placing the elements along a line and this is the type of configuration we will look into first.

2.3.2 Bandwidth broadening by using Arrays

So far we have only looked at a single frequency, but the SKA project requires multiple frequencies to be observed at the same time. Single dipole antennas have limited bandwidth, in the order of 14% as stated earlier, but with dipole arrays much larger bandwidths are obtained.

These arrays might provide the necessary increase in bandwidth and thus we study it further by analysing different configurations. The log-periodic antenna structures introduced by DuHamel and Isbell [12] shows very promising results and will receive more attention. The antenna size is also of importance and we look at ways to reduce the antenna's size physically without affecting its electrical performance.

2.4 Theory of Frequency Independent Antennas

Before 1950, wideband antennas generally had bandwidths of 2:1, then after that a new type known as frequency-independent antennas were introduced. These antennas extended the achievable bandwidth; 40:1 and even more were realistic and this was possible by specifying the geometries by angles. These antennas were mostly used in the 10 MHz to 10 GHz frequency band and can be used on a variety of applications such as TV, feeds for reflectors and lenses and point-to-point communication. These applications would generally only use a portion of the antenna's bandwidth, thus making it very ineffective, but the same antenna can be used for different applications. As far as the author knows only one application namely for electronic warfare would use such wide bandwidths.

Antenna scale modelling can be applied to frequency independent antennas. The electrical characteristics, such as input impedance, radiation pattern, polarisation, and so forth, are invariant to a change in the physical size of the structure. However this does require a similar change in the operating frequency. For instance, if all the physical dimensions are increased by a factor of 2, the performance of the antenna will stay the same if the frequency is decreased by a factor of 2.

The scaling characteristics indicate that if the antenna is completely specified by angles, its performance will be frequency independent according to Rumsey [16].

The treatment of the frequency independent antennas presented here is taken from Balanis [1] and is very similar to the work done by Rumsey [16] and simplified by Elliot [17].

One describes the geometry of the antenna with spherical coordinates (r,θ,ϕ) that has both terminals at the origin. Further assumptions are that the antenna is perfectly conducting and surrounded by an infinite homogeneous medium. The surface or edge of

the surface can be described by a curve

$$r = F(\theta, \phi) \tag{2.9}$$

where r represents the distance along the edge of the surface. The antenna can now be scaled in order to achieve different frequency bands. If the antenna is scaled K times higher than the original frequency, the physical surface of the antenna must be made K times smaller in order to maintain the same electrical performance for the new frequency. The new surface can be described by

$$r' = KF(\theta, \phi). \tag{2.10}$$

The new and old surfaces are identical in shape but only differ in size. This difference in size corresponds directly to an inverse difference in operating frequency of the antenna. The spiral antenna analysed next serve as an example for frequency independent antennas [1].

2.5 Spiral Antennas

The equiangular spiral is one geometry which can be described by angles. It is necessary to specify the arm length in order to have a finite antenna as the spiral curve extends to infinity. The low frequency cut-off is when the wavelength is comparable to the arm length. The radiation pattern and impedance characteristics are independent of frequency above this point [1]. In practice the high frequency cut-off has usually to do with the feeding or manufacturing tolerances associated with the antenna.

2.5.1 Planar Spiral

The shape of the equiangular spiral is given in polar coordinates as

$$r = ae^{b\theta} \tag{2.11}$$

with a being the inner radius of the spiral and b the rate of expansion. In Cartesian form it is

$$x = ae^{b\theta}\cos\theta \tag{2.12a}$$

$$y = ae^{b\theta}\sin\theta \tag{2.12b}$$

Another interesting spiral is the Archimedean spiral which is given by

$$r = a + b\theta \tag{2.13}$$

in polar coordinates with a and b having the same meaning as for the equiangular spiral. In Cartesian form it is

$$x = (a + b\theta)\cos\theta \tag{2.14a}$$

$$y = (a + b\theta)\sin\theta \tag{2.14b}$$

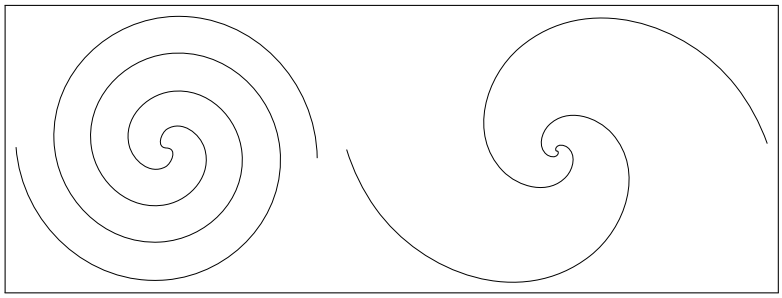

Figure 2.2: An Archimedean (left) and equiangular (right) spiral.

Figure 2.2 shows examples of Archimedean and equiangular spirals. One spiral arm is drawn as the positive feed and then a flipped version is added as the negative feed for the antenna that is fed in the centre of the spiral. The antenna is placed in the xy-plane and then radiates in the positive and negative z-directions.

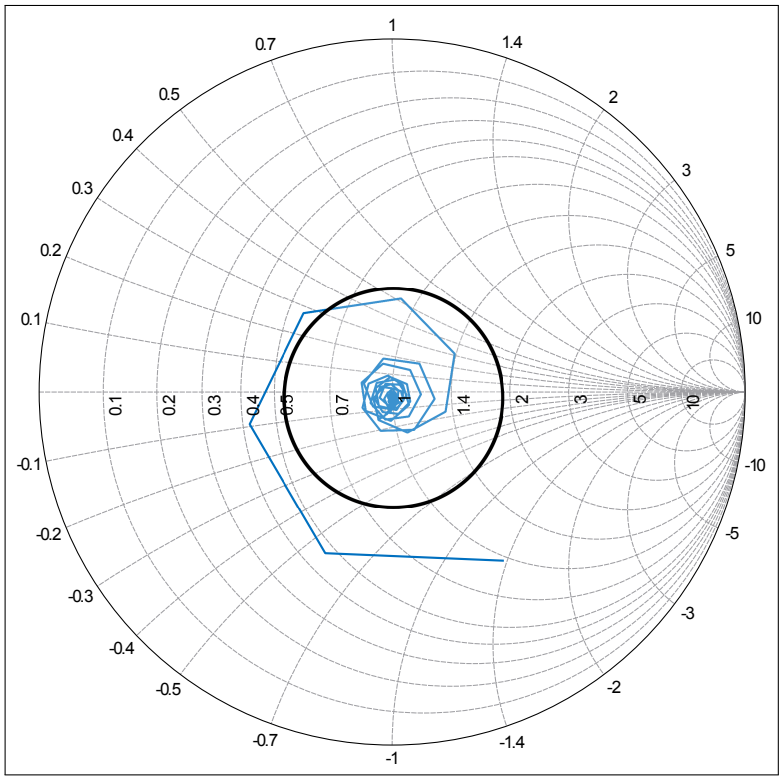

Figure 2.3: Smith chart of an Archimedean spiral antenna (f_{low} outside circle and f_{high} in centre).

The surface current for the high frequencies are close to the origin of the spiral and this produces the radiated fields. As the frequency lowers the currents move outward along the spiral and keeps on radiating. If the spiral started infinitely small at the centre and the arms extended to infinity the antenna would have infinite bandwidth. Practically the

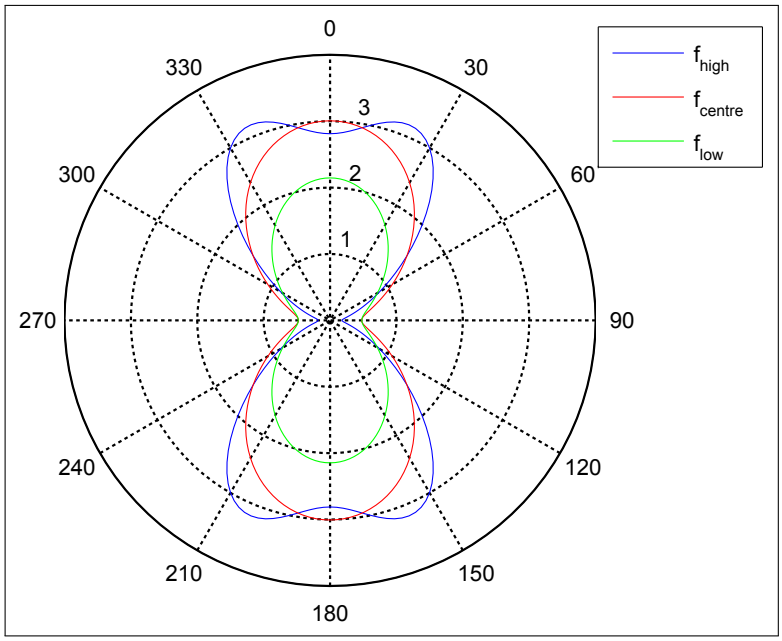

Figure 2.4: Polar patterns of an Archimedean spiral antenna at $\phi = 0$.

antenna does not start infinitely small at the centre and the arms do not extend to infinity. These two restrictions provide the upper and lower cut-off frequencies for the spiral.

An Archimedean spiral with four turns was simulated in FEKO. We chose a wire configuration as this resulted in faster simulation time. Spiral plate and slot antennas could also be simulated, but would result in much slower simulations.

Figure 2.3 shows a Smith chart with the reflection coefficient for this wire spiral antenna. The blue line represents the reflection coefficient and the black circle the -10 dB reflection limit. For this wire antenna, the normalised impedance is set at 600 Ω with a wire radius of 0.1 mm. Lower impedances are obtainable by using a thicker wire element (a wire radius of 1 mm produced almost the exact same results with a normalised impedance of 325 Ω) or by using a flat plate for the arms. Measured values of 75-100 Ω input impedance were obtained by Dyson [18] who used spiral plates. The reflection coefficient starts in the centre of the chart (Figure 2.3) at the high frequencies and as the frequency lowers, the reflection coefficient rotates outward from the centre. The lowest frequency that the antenna radiates at is when the diameter of the spiral is about half a wavelength. At this point the reflection coefficient moves out of the -10 dB circle and instead of radiating, the energy gets reflected back to the source.

The upper frequency limit seems to be infinite when observed from the Smith chart, but this limit is reached when we look at the radiation pattern in Figure 2.4. Here we observe a polar pattern cut of the radiated field of the spiral antenna at the upper, middle and lower parts of the bandwidth of the antenna. The red line shows the wanted radiation

pattern over the entire bandwidth of the antenna. The green line shows the same pattern, but is smaller, as the reflection increases at the lower frequencies. The blue line shows the radiated field at the high frequencies and here the pattern starts to deform. Instead of having two major lobes, each lobe splits and form two lobes directed away from each other. This deforming in the radiation pattern we consider as the upper frequency limit as the antenna produces unwanted radiation patterns.

This antenna is circularly polarised and for a spiral that rotates clockwise as in Figure 2.2 produces two different lobes. The top radiation lobe has a left-hand-circular (LHC) polarisation and the bottom lobe has a right-hand-circular (RHC) polarisation.

Thus far the spiral has remained planar, but we intend to inspect and analyse what would happen if we introduced another dimension to the spiral. This leads to a non-planar structure which could be configured in a number of ways. One specific configuration we will analyse is the conical spiral antenna.

2.5.2 Conical Spiral

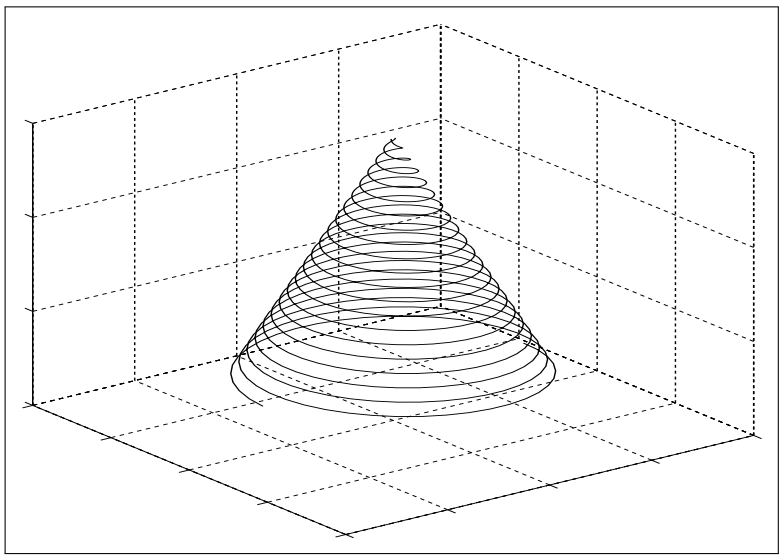

Figure 2.5: Conical spiral: Archimedean spiral wrapped around a cone.

The conical spiral can be described as a planar spiral wrapped around a conical surface as shown in Figure 2.5. The equation that describes this spiral is given in Cartesian form as

$$x = (a + b\theta)\cos\theta \tag{2.15a}$$

$$y = (a + b\theta)\sin\theta \tag{2.15b}$$

$$z = c\theta \tag{2.15c}$$

which is the same as equations 2.14(a-b) but with a z-dependency. The parameter c relates to the height of the cone. With this parameter chosen as zero, the planar spiral is gained. When it is increased, the height of the cone increases and the spiral is wrapped around this cone. When c is large, the cone is long and thin and the spiral is wrapped loosely around the cone. When c is small, the cone is short and fat and the spiral is wrapped tightly around the cone. If a negative value is chosen for c, the cone will be directed downwards, instead of upwards, for positive values.

A major difference between the planar and conical spirals is that the planar spiral provides two radiation lobes, while the conical spiral only provides one (unidirectional) towards the apex of the cone. The polarisation and impedance stays the same for both types of spirals. Conical spirals can be flush-mounted on a ground plane, but this results in a reduction of bandwidth [1].

2.6 Log-Periodic Antennas

The log-periodic structure is a configuration that is very close to the frequency independent concept and was introduced by DuHamel and Isbell [12]. The entire shape can't only be described by angles, thus it is not exactly frequency independent.

2.6.1 Planar and Wire Surfaces

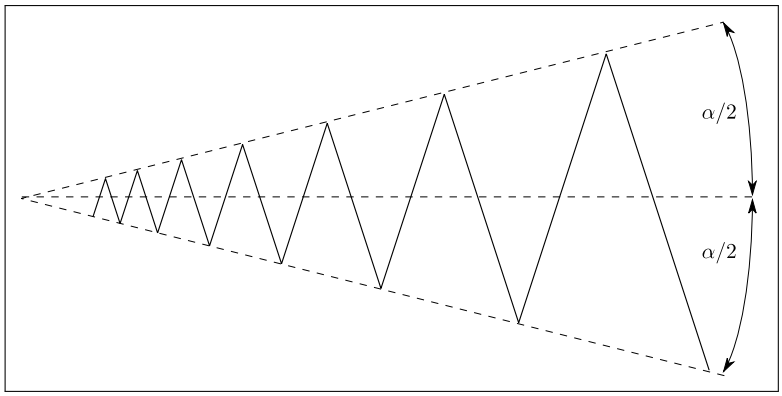

Figure 2.6: Log-periodic configuration. Redrawn from Balanis [1].

Figure 2.6 shows a log-periodic structure. This configuration consists of a thin metal strip whose edges are specified by $\alpha/2$ and a distance characteristic is needed to specify the length from the origin to a point on the structure.

The shape of the structure can be given in spherical coordinates as

$$\theta = \text{periodic function of } [b \ln(r)] \tag{2.16}$$

and an example of this is

$$\theta = \theta_0 \sin[b \ln(r/r_0)] \tag{2.17}$$

with θ_0 a constant and the values of θ are repeated when the radial frequency's logarithm ($\ln(\omega)$) changes by $2\pi/b$. The logarithm of the frequency then produces a performance that is periodic; thus forming the name *log-periodic* or *logarithmic-periodic*.

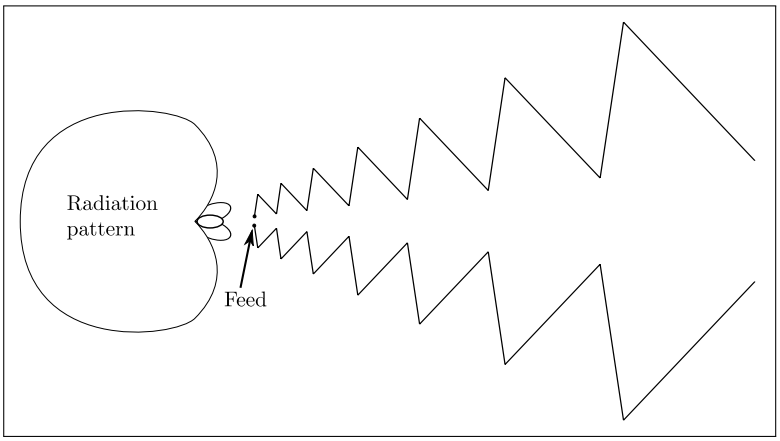

Figure 2.7: Log-periodic antenna. Redrawn from Balanis [1].

Figure 2.7 shows a log-periodic antenna configuration. It consists of two log-periodic structures as shown in Figure 2.6 and is fed on the left. The radiation pattern is unidirectional as shown with some minor side lobes. The main beam is linearly polarised and directed towards the apex formed by the two structures. The radiation pattern of this type of structure is not completely frequency independent, but the amplitude variation can be very small for some designs that they are practically considered as frequency independent. In order to keep the amplitude variation small over the entire frequency band, enough dipoles are needed for the antenna. The exact number of how many dipoles are enough relates to the bandwidth that needs to be covered. For a 4:1 bandwidth the geometric ratio τ needs to be about 0.9 which directly affects the number of dipoles and gives about 20 elements. The variation in directivity is then about 1 dB and if fewer elements are present, the variation in directivity becomes larger. This will be shown more clearly in Chapter 3 when design curves are generated.

Log-periodic antennas made of wires were introduced by DuHamel [12]. DuHamel investigated the current distribution on planar log-periodic antennas as shown on the left in Figure 2.8. He discovered that the fields on the planar structure attenuated quickly with distance away from the edges and this suggested a strong current concentration at the edges of the planar structure. He then predicted that if the inner surface is removed to form the wire structure as in Figure 2.8, the performance of the antenna should

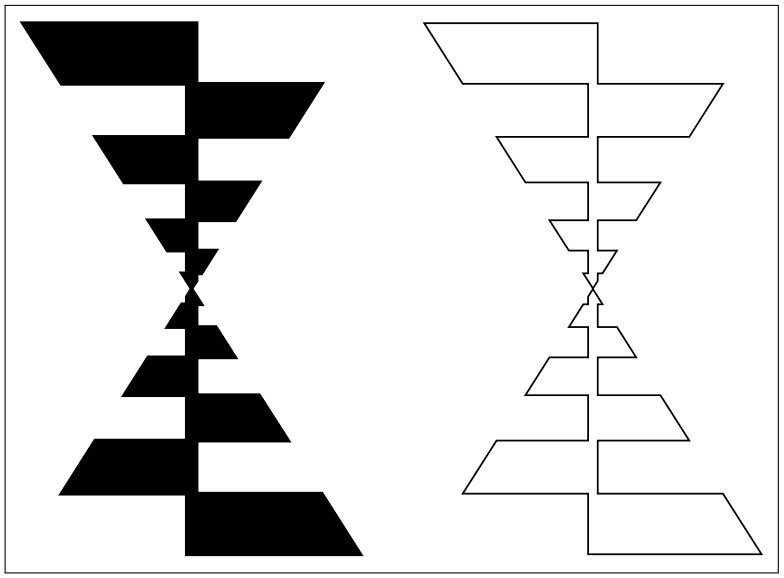

Figure 2.8: Planar (left) and wire (right) trapezium shaped tooth log-periodic antennas. Redrawn from Balanis [1].

not change significantly. This was investigated and a wire antenna with an identical geometric shape to the planar structure was built. He found, as predicted, that the performance of these two antennas were very similar; thus discovering a much simpler, cheaper, lighter and less wind resistant antenna [1]. This is of great importance for the whole SKA project as antenna costs needs to be low, to fit into the budget. Wind resistant antennas are also favourable as they need to withstand wind and not deform.

The teeth of Figure 2.8 form a geometric ratio which we define for this structure as

$$\tau = \frac{R_n}{R_{n+1}} \tag{2.18}$$

where R_n represents the distance from the origin to the n'th tooth and R_{n+1} the tooth after that. This parameter defines the period of operation for the antenna and if two frequencies (f_1 and f_2) are set apart by one period, the relation of these frequencies are given by τ.

$$\tau = \frac{f_1}{f_2}, \quad f_2 > f_1 \tag{2.19}$$

Extensive studies have been done on these wire antennas as a function of their geometrical parameters. The performance of these structures were very similar to the planar and conical structures. The most notable difference is that the spiral antennas are circular polarised while the log-periodic antennas are linearly polarised.

2.6.2 Dipole Arrays

The LPDA was introduced by Isbell [13] and looks similar to the Yagi-Uda antenna. This LPDA consists of a number of linear dipoles placed next to each other in order to form a

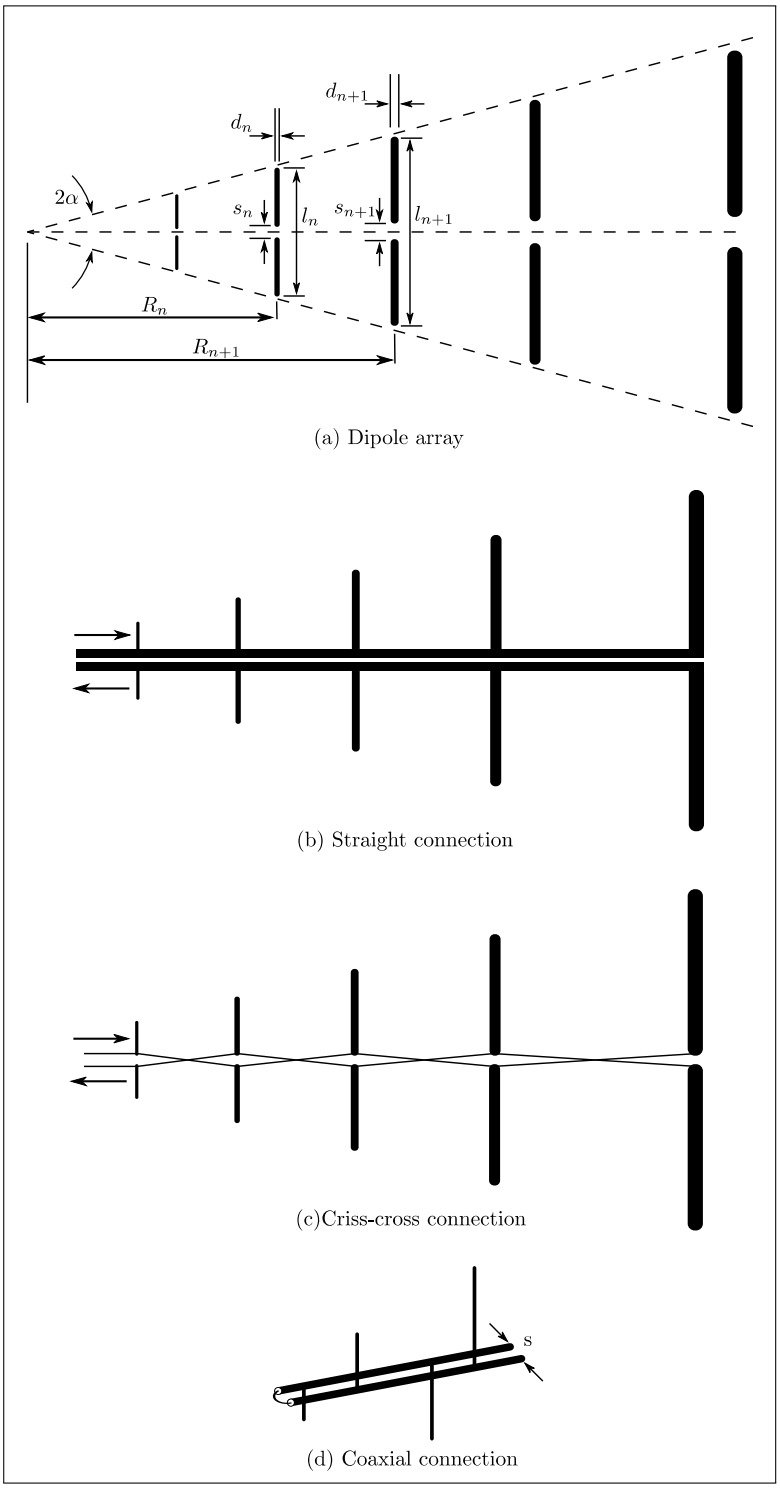

Figure 2.9: LPDA and possible connections for the LPDA. Redrawn from Balanis [1].

coplanar array as shown in Figure 2.9(a). This antenna can achieve similar directivities as the Yagi-Uda does, but can operate over a much wider bandwidth and has several other differences.

The geometrical dimensions of the Yagi-Uda antenna does not follow any set pattern, but the LPDA does. The lengths (l_n's), spacings (R_n's), diameters (d_n's) and the gap spacings at the dipole centres (s_n's) increase logarithmically for the LPDA by the inverse of the geometric ratio τ and is

$$\frac{1}{\tau} = \frac{l_2}{l_1} = \frac{l_{n+1}}{l_n} = \frac{R_2}{R_1} = \frac{R_{n+1}}{n} = \frac{d_2}{d_1} = \frac{d_{n+1}}{d_n} = \frac{s_2}{s_1} = \frac{s_{n+1}}{s_n} \tag{2.20}$$

The spacing factor σ is associated with this array and is given by

$$\sigma = \frac{R_{n+1} - R_n}{2l_{n+1}} \tag{2.21}$$

When straight lines are drawn through the ends of the dipoles they meet and form the angle 2α which is a quality of frequency independent structures.

It is difficult to maintain the spacings at the dipole centres and dipole diameters, thus we keep them constant. These minor adjustments simplify the antenna construction and does not degrade the performance of the antenna significantly.

Only one element is fed with the Yagi-Uda antenna while the rest of the elements are parasitic. This is opposed to the LPDA where all of the elements are fed. Figure 2.9(b) and 2.9(c) shows two basic methods of feeding this antenna and both are done at the small end of the antenna.

In Figure 2.9(b) the phase relationship for the current is the same in all of the elements. If the elements are close to one another the phase of the current advances to the right and produces a major radiation lobe towards the longer elements which interferes with the lobe.

By criss-crossing the feed line between the elements as shown in Figure 2.9 we add 180° phase to each element. Now two adjacent elements are about 180° out of phase with each other which results in a very small amount of energy that gets radiated which means the interference effects are very small. By reversing the phase the elements produces a beam towards the apex of the structure. The most active elements are the ones that are near resonance (also referred to as the active region) and produces a radiation pattern towards the vertex of the antenna [1].

This means that a straight connection as in Figure 2.9(b) is undesirable and will result in unwanted radiation patterns due to higher order modes excited on longer dipoles. The criss-cross connection as in Figure 2.9(c) is much more desirable and results in a stable radiation pattern.

The feed for Figure 2.9(c) is very convenient for a balanced line like a two-conductor transmission line. Figure 2.9(d) shows a practical feeding method in order to obtain the 180° phase difference between elements if a coaxial cable is used to feed the antenna. This feed forms a built-in broadband balun which balances the whole system. The outside conductor is connected to the feeder line of the antenna and the inner conductor is extended and connected to the other feeder line.

In order for this structure to be a true log-periodic array it would have to be infinite. Thus it is truncated at both ends in order to provide a practical broadband antenna. This truncation limits the operating frequency from infinite to a certain bandwidth.

The upper and lower cut-off frequencies can be determined by the shortest and longest dipoles of the antenna. The lower cut-off is when the longest dipole is about $\lambda/2$ of the lower limit of the bandwidth. The upper frequency cut-off is when the shortest dipole is about $\lambda/2$ of the upper limit of the bandwidth. The active elements or also called the active region is when the dipoles are about $\lambda/2$. This active region moves from the longer elements to the shorter elements as the frequency increases. This means that the phase centre of this antenna moves as the frequency changes which is unwanted in reflector and lens antennas [1].

2.6.3 Design of Dipole Array

The goal of designing an antenna is that it must meet a specification. Carrel [2] provides an introductory and practical design method for an LPDA antenna. He has also compiled a set of curves to aid us in this design. The parameters τ, σ and α describe the LPDA configuration and are related by

$$\alpha = \tan^{-1}\left(\frac{1-\tau}{4\sigma}\right) \tag{2.22}$$

If two of these parameters are specified, the third parameter can be calculated. Figure 2.10 shows directivity curves as a functions of τ and σ. The contours with τ values lower than 0.8 have been extrapolated from the rest of the contours.

Please note that these curves in Figure 2.10 were calculated incorrectly at first by Carrel [2], but corrected by Butson [19]. A $\sin(\theta)$ function was placed in the numerator instead of the denominator and resulted in directivities of 1-2 dB too high. This has been corrected and the more accurate values are shown in Figure 2.10.

2.6.4 Carrel's design equations

We now introduce a number of Carrel's [2] equations to aid us in the design of an LPDA antenna.

The shortest and longest lengths of the dipoles determine the bandwidth of the antenna.

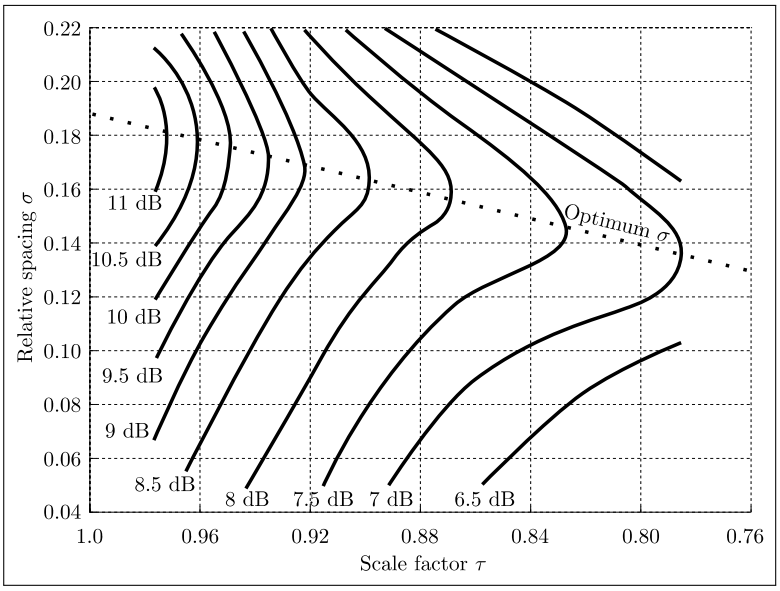

Figure 2.10: Computed contours of constant directivity versus σ and τ for log periodic dipole arrays [2]. Redrawn from Balanis [1].

The active region is determined by the specific design that is used. The bandwidth of the active region (B_{ar}) is determined by α and τ in

$$B_{ar} = 1.1 + 7.7(1-\tau)^2 \cot\alpha \tag{2.23}$$

A larger bandwidth is usually obtained than what is required and these two parameters are related by

$$B_s = BB_{ar} \tag{2.24}$$

with B_s being the designed bandwidth, B the required bandwidth and B_{ar} the active region of the bandwidth.

The length of the structure is given by

$$L = \frac{\lambda_{max}}{4}\left(1 - \frac{1}{B_s}\right)\cot\alpha \tag{2.25}$$

with L being the total length and $\lambda_{max} = 2l_{max}$ with l_{max} being the longest element.

The number of dipoles (N) in the array is calculated by

$$N = 1 + \frac{\ln(B_s)}{\ln(1/\tau)} \tag{2.26}$$

The spacing s between the conductors of the feeder line is determined by the diameter of the dipoles and the feeder line self and the required input impedance. We define the characteristic impedance Z_a of the dipoles by

$$Z_a = 120\left[\ln\left(\frac{l_n}{d_n}\right) - 2.25\right] \tag{2.27}$$

with l_n/d_n being the length-to-diameter ratio for the nth dipole. Ideally this ratio should be the same for all the dipoles, but practically these dipoles can be divided into subgroups of the same diameter.

Figure 2.11 shows the effective loading that the dipole elements have on the feeder line.

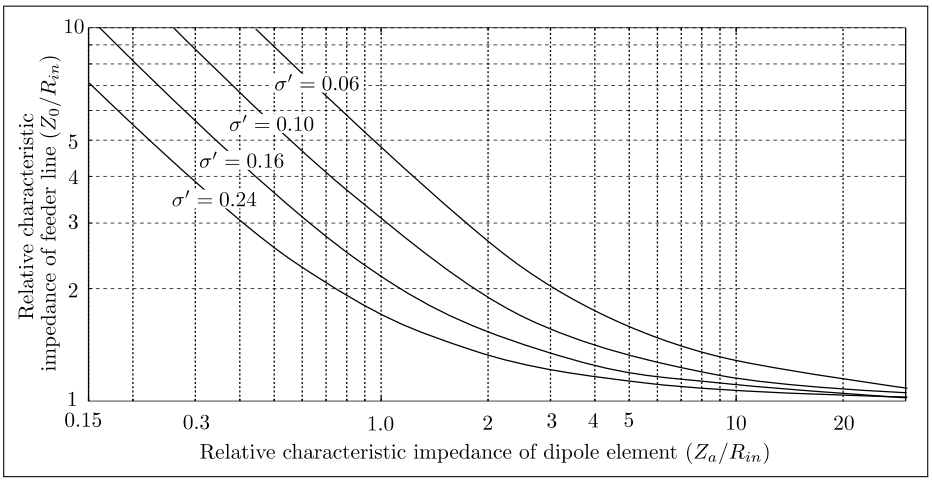

Figure 2.11: Relative characteristic impedance [2]. Redrawn from Balanis [1].

Here $\sigma' = \sigma/\sqrt{\tau}$ is the relative mean spacing, Z_a is the average characteristic impedance of the dipoles, R_{in} the input impedance and Z_0 the characteristic impedance of the feeder line. The spacing s between the two conductors of the feeder line is

$$s = d \cosh\left(\frac{Z_0}{120}\right) \tag{2.28}$$

with d being the diameter of the feeder line.

2.6.5 Carrel's design procedure

Carrel's design procedure is given now and is based on the design equations as stated above. This procedure assumes that the directivity be specified in dB, the input impedance be real (R_{in}), the diameter of the feeder line (d) and the cut-off frequencies of the bandwidth be given. With all of these parameters given, the procedure is as follow:

1. With D_0 (dB), use Figure 2.10 and find σ and τ.
2. Use equation 2.22 to calculate α.
3. Use equations 2.23 and 2.24 to calculate B_{ar} and B_s.
4. Use equations 2.25 and 2.26 to calculate L and N.
5. Use equation 2.27 to calculate Z_a and $\sigma' = \sigma/\sqrt{\tau}$

6. Use Figure 2.11 to find Z_0/R_{in}.

7. Use equation 2.28 to calculate s.

This concludes Carrel's design as given in Balanis [1] and an example of this design is done in Appendix A.

2.7 Typical Performance of LPDA

The largest part of the design of this type of antenna is now complete and we want to know what the typical results are that we can expect.

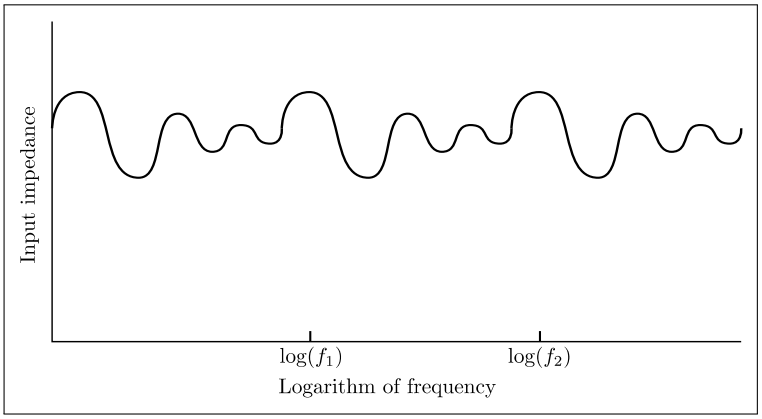

Figure 2.12: Expected variation of the input impedance for an LPDA antenna as a function of the frequency. Redrawn from Balanis [1].

When we plot the input impedance as a function of frequency a repetitive pattern emerges. If we then take the logarithm of this frequency, it becomes periodic as in Figure 2.12 with each cycle repeating itself. Other antenna parameters such as the radiation pattern, directivity, beamwidth and side lobes undergo the same periodicity.

This periodicity does not provide broadband operation for this antenna, but if the variations in the impedance, radiation pattern, directivity, and the rest of the parameters are small enough, it is considered to have broadband operation.

The geometric ratio determines the frequency span Δ of each cycle. This parameter can be defined by the logarithm of τ and is

$$\Delta = \ln(f_2) - \ln(f_1) = \ln(1/\tau) \tag{2.29}$$

The changes that happen within each cycle ($f_1 \leq f \leq f_2$ with $f_2 = f_1/\tau$) repeat at the rest of the bandwidth just by replacing the subscripts (1) and (2) with $(n-1)$ and (n) respectively with n being the dipole number.

Typical LPDA designs have geometric ratios of 0.7 to 0.95 ($0.95 \geq \tau \geq 0.7$) and apex half angles between 10° and 20° ($20° \geq \alpha \geq 10°$). The relation between these two parameters are that when α increases, τ decreases and vice versa. Larger values of α result in more compact structures which require less dipoles with larger spaces in-between. Opposite to this, smaller values for α results in more dipoles that are closer together. More dipoles means more dipoles that are in the active region which results in a smoother frequency response.

Figure 2.13 shows the typical performance for commercial LPDA antennas. The gain decreases rapidly at the lower end of the frequency band and stays stable for the rest of the band. The VSWR stays under two for the whole bandwidth. The E- and H-plane beamwidth differ a lot, meaning that the pattern is oval and not round in shape, but at the high frequencies it becomes almost round [1].

2.8 Antenna Size Reduction

The structures we have analysed thus far can become quite large when working at low frequencies. Thus we aim to reduce the structures physical size, while still maintaining the same frequency response.

Sharma [5] provides a possibility of reducing the zig-zag structure's height by folding it. He shows the folding of the longer antenna elements onto itself and the related changes in antenna characteristics. His idea is that by doing this one can reduce the size of the antenna while the antenna characteristics remain mostly unchanged. His article was found to be quite difficult to understand and thus a similar process will be carried out in Chapter 4 with the aim of making things clearer.

2.9 Recap

In this chapter the following was discussed:

1. the infinitesimal dipole,
2. the half-wavelength dipole and its radiation characteristics
3. dipole arrays
4. the theory of frequency independent antennas
5. spiral antennas
6. log-periodic antennas and a design procedure
7. typical results expected for LPDA antennas

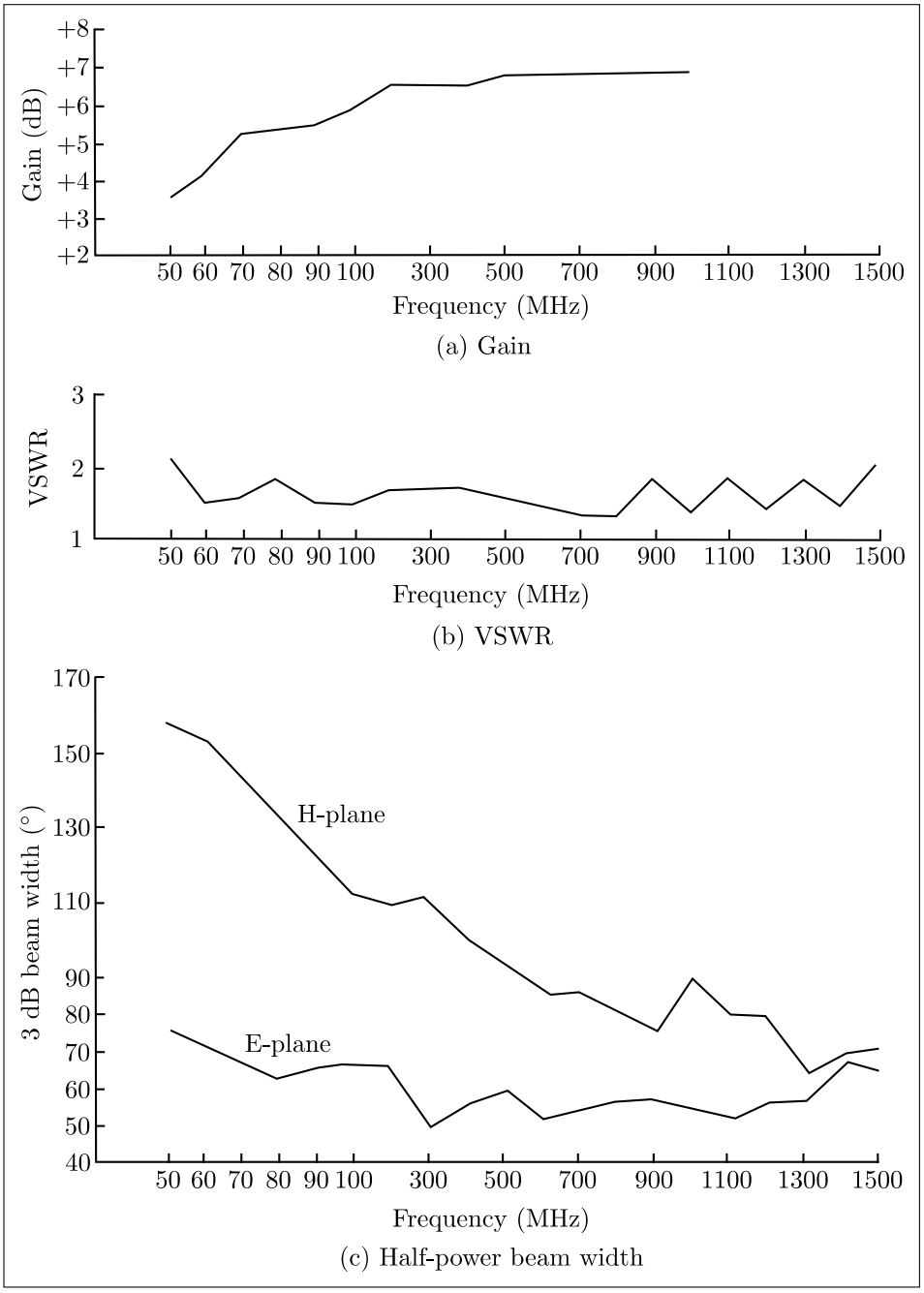

Figure 2.13: Typical gain, VSWR and half-power beamwidth to be expected for commercial LPDA. Source: American Electronic Laboratories [3]. Redrawn from Balanis [1].

8. miniaturising of LPDA antennas by folding them

Chapter 3

Printed LPDA Parameter Study and Design

3.1 Introduction

This chapter presents a parameter study for a printed LPDA antenna. This study concludes by building a scale model antenna and measuring it.

The aim of this chapter is to discover which parameters influence the LPDA's performance and in what way. This will be done by using the design parameters σ, τ, and α which provides the general configuration of the LPDA. Design curves are generated to show the effects on the characteristics of the LPDA due to the change in the design parameters. We use the wire design by [2] and convert it straight to microstrip for the printed structure.

This study was carried out through simulation and the results processed. Very careful thought has gone into the selection of the preferred package for this type of problem. FEKO was chosen as the simulation software to be used and the reasons for this selection will be discussed next.

3.2 Simulation Selection

In the computational electromagnetic community there exist a few methods of simulating RF and microwave structures. All of these methods have to solve Maxwell's equations which are written in differential form as:

$$\nabla \times \vec{E} = -\frac{d\mu\vec{H}}{dt} \tag{3.1}$$

$$\nabla \times \vec{H} = J + \frac{d\epsilon\vec{E}}{dt} \tag{3.2}$$

$$\nabla \cdot \epsilon\vec{E} = \rho \tag{3.3}$$

$$\nabla \cdot \mu \vec{H} = 0 \tag{3.4}$$

The numerical approximation of Maxwell's equations is known as computational electromagnetics (CEM). The applications of CEM are quite vast and include antennas which we will focus on.

The most widely used methods are the finite difference time domain (FDTD) method, the method of moments (MoM), and the finite element method (FEM). These methods all require some sort of discretisation (also known as meshing) of some electromagnetic property. For the MoM it is the surface current and for FDTD and FEM it is the E-field according to Davidson [20]. Software packages that use these methods are shown in Table 3.1.

Table 3.1: CEM methods with commercial software examples

Method	Equation type	Domain	Software package example
MoM	Integral	Frequency	FEKO
FDTD	Differential	Time	CST Microwave Studio
FEM	Differential	Frequency	Ansoft's HFSS

Many other software packages also exist and are commercially available. FEKO and CST are however available and known to the author and have been used with successful results in the past, thus a choice between these two will be made on which is preferred for this thesis. (Please note that HFSS was originally from Ansoft, but has been bought by Ansys.)

3.3 FDTD compared to MoM

FDTD (of which CST is an example) and MoM (of which FEKO is an example) can produce very much the same results when they both run a simulation, but the way in which they do it is the big difference.

MoM mesh the surface of structures and calculates the current on all segments (for wires) and patches (for surfaces). This is done by setting up an integral matrix equation which leads to a set of linear equations. For antenna problems one would expect the matrix dimension to range from a couple hundred to several thousand. The upper bound for this is usually due to computational limitations in the form of not enough memory (RAM) or excessive simulation run-time.

FDTD on the other hand meshes the whole volume of a structure into a three-dimensional grid. Here the E-field in each grid element is determined by the previous values of this element and its adjacent neighbours by solving a discrete differential equation. The amount of elements can be quite immense and range typically from several thousand

to several million elements. The upper bound for this has also to do with the amount of memory (RAM) available and the run-time [20].

3.3.1 Strong and weak points of MoM

The strong and weak points of the MoM (this implies FEKO) is now given in order to help make the best decision.

The strong points are the following.

- The MoM treats perfectly conducting surfaces efficiently by only meshing the surface and not the surrounding air.
- The current density is the important variable from which the antenna parameters (radiation pattern, impedance and so forth) are calculated.
- The meshing is flexible - meaning different areas can have different mesh sizes.

The weak points are the following.

- The MoM does not handle dielectrics very well as it uses integration, when differentiation works better.
- It does not scale well with frequency. For a surface mesh (2 dimensional) this implies that the scaling is of the order 6 which if the frequency is doubled could result in the simulation run-time to be 64 times as long. The order of scaling for a wire mesh (1 dimensional) is 3 while for a volumetric mesh (3 dimensional) it is 9.

To sum this up, the MoM works well when highly conducting surfaces or wires are present. If inhomogeneous dielectrics are present it is likely to be computational expensive [20]. Another important consideration is that this is done in the frequency domain, thus for wide band applications many frequency points needs to be simulated.

3.3.2 Strong and weak points of FDTD

The strong and weak points of the FDTD (this implies CST) is now given in order to aid in the selection process.

The strong points are the following.

- This is a very simple implementation. One can implement this method self in a reasonable time as compared to the MoM or FEM.
- The FDTD operates in the time domain and thus wideband data are possible to acquire from a Fourier transform with a single run.
- The handling of inhomogeneous materials is very good.

- It scales reasonably well with frequency. The order of scaling is 5.5 which is slightly better than MoM order of six for surfaces. If compared to the MoM volume order of scaling, which is nine, this scaling of 5.5 is much better.

The weak points are the following.

- The FDTD is not as efficient as the MoM when working with only perfectly conducting surfaces.
- The meshing is not as flexible as MoM - with flexible grids this method loses much of its simplicity.

To sum this up, the FDTD works well with wideband structures and handles inhomogeneous dielectrics with ease [20].

So far we are not yet clear on which method and corresponding software to use. The antenna that needs to be simulated will be discussed in Chapter 4 in detail, but it can already be said that it will need to operate over a wide band and be constructed of wire. The FDTD handles wideband structures very well with a single run compared to the multiple runs of the MoM. The MoM again handles wire structure very well and does not need to mesh the surrounding air as the FDTD method has to. To see which of these two methods are best for this specific problem, they are compared to each other by using FEKO and CST.

3.4 CST compared to FEKO

CST and FEKO are excellent software packages and here they will be compared to each other for a specific problem. Here the same antenna (Carrels design example) will be simulated in both software packages and the results compared to each other. Seeing as this is the same antenna one expects the same result. The actual test is to see which package simulates it the fastest.

Both simulation packages were simulated and the comparisons are now given in terms of the reflection coefficient and the radiation pattern.

Figure 3.1 shows the comparison of the reflection coefficient for these two software packages. Very similar results are obtained as can be clearly seen, thus it means the two software packages produce similar result in terms of the reflection coefficient.

Figure 3.2 shows the comparison of the directivity for these two software packages. Very similar results are obtained again as can be clearly seen. This means the two software packages produce similar result for both the reflection coefficient and directivity.

With the results being the same, the choice between these two now fall on the simulation

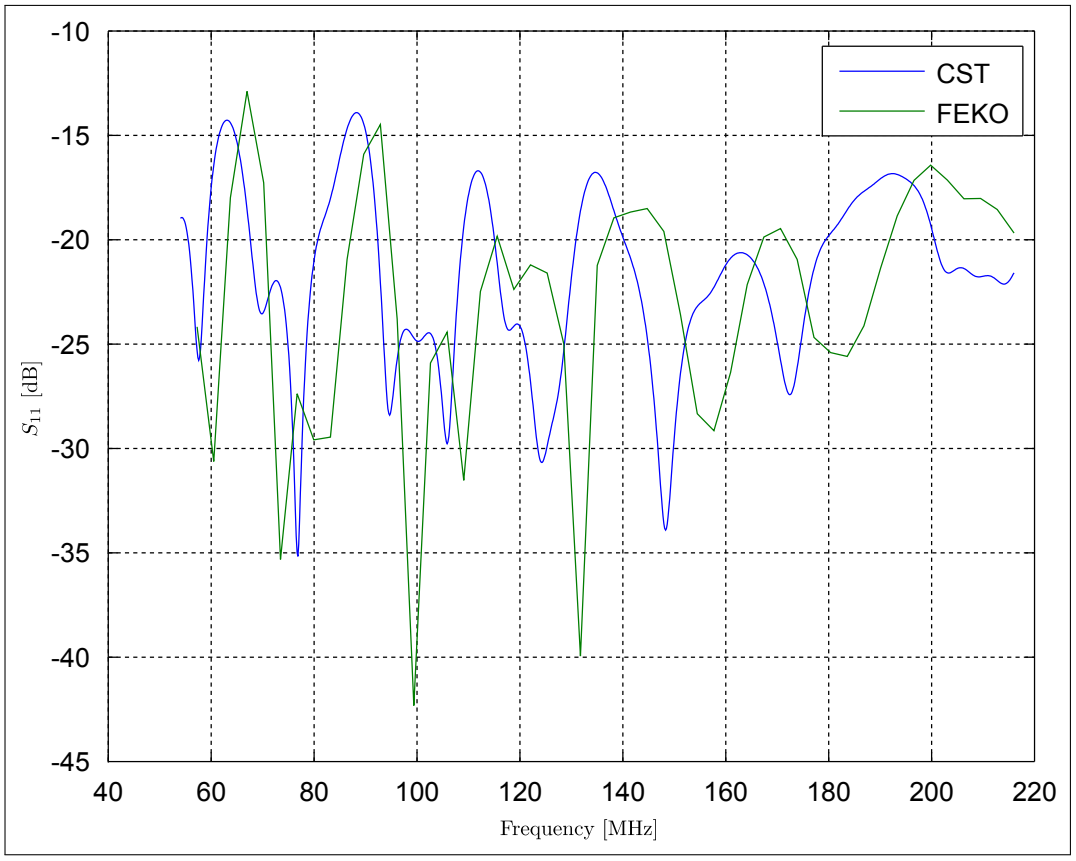

Figure 3.1: Comparison of the reflection coefficient for an example antenna between CST and FEKO.

time for these two packages. Both simulations were done on the same quad-core PC with 8 GB RAM. Table 3.2 contains the important relevant information for this decision.

Table 3.2: Simulation comparison between CST and FEKO.

Software	Mesh size	Memory Used (RAM)	Simulation time used
CST	940 000 Meshcells	192 MB	$\approx$ **33 minutes**
FEKO	816 Segments	13.6 MB	$\approx$ **9 minutes**

Here we clearly see that FEKO is the better solution for this problem. The simulation time is shorter by more than a factor of three. CST used one run in the time domain and then Fourier transformed into the frequency domain while FEKO used 100 frequency points in order to achieve the results. Another important parameter to take into account is the RAM that was needed for this run. FEKO used less than a tenth of what CST used and thus means it requires far less RAM for the same simulation. This means that CST is much more computational expensive for this specific problem and thus the choice is made to use FEKO as the software package for this thesis.

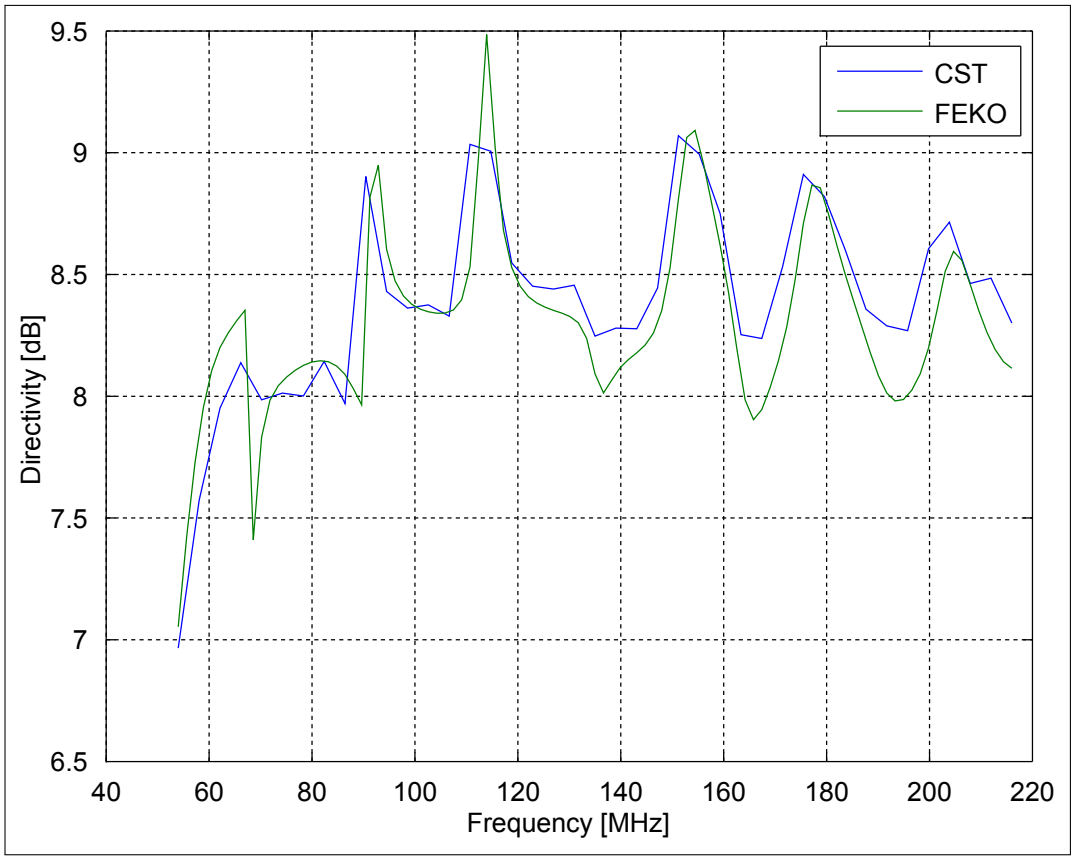

Figure 3.2: Comparison of the directivity for an example antenna between CST and FEKO.

Also note that the FEM (which Ansoft's HFSS is an example of) also needs to mesh the whole volume as the FDTD does. This suggests similar mesh sizes along with similar simulation times for CST and HFSS. This is further a problem as HFSS operates in the frequency domain and thus several runs will need to be executed. This leads us to believe that FEKO will still be computational cheaper than HFSS.

3.5 Model

Now that FEKO has been chosen as the software package to use one needs to implement the model of the antenna in the software. The same design procedure of Carrel was taken, but it was decided to use flat surfaces instead of wires. This choice is made as the idea is to produce a scale model printed LPDA on a substrate in this Chapter. In the next Chapter we look at a wire structure without any dielectric. Furthermore it was decided to use two LPDA antennas in a non-planar configuration as shown in Figure 3.3 by Dubrovka et al. [4] as this provides some adjustments of the beamwidth. The model is coded in EDITFFEKO to be drawn quickly and easily with the added functionality of changing parameters. This method is chosen as the geometry of the structure can easily be coded. CADFEKO is also a possibility, but without scripting capabilities it will

complicate the drawing of the structure. With EDITFEKO only a parameter needs to change and the whole structure will be drawn which is the main reason for this decision.

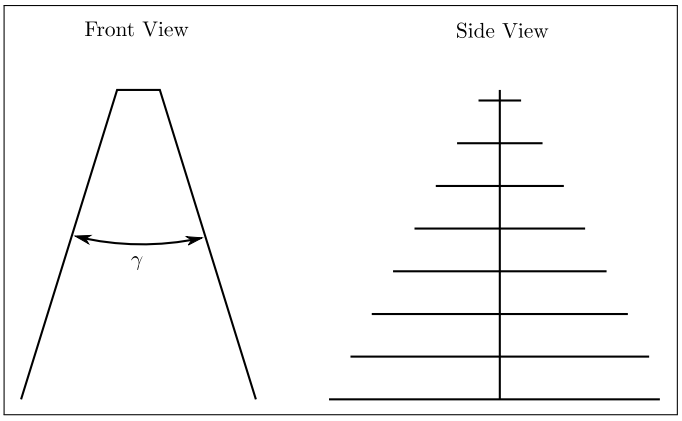

Figure 3.3: The non-planar LPDA antenna. Configuration redrawn from Dubrovka [4].

The whole structure is drawn piece by piece by implementing a command in a loop with the correct parameters. This results in the whole structure being drawn quickly and efficiently. Mesh refinement is easily done here by changing the mesh sizes according to the length of each dipole. The longer dipoles have larger meshes as low frequencies gets radiated here and the shorter dipoles have smaller meshes as high frequencies gets radiated here and does not continue along the feed line to the longer dipoles.

The model is simulated and the data stored for later processing with MATLAB. The model stays the same and the parameters τ, α and F_a (Roundness factor) are adjusted. With each simulation the model receives a unique name and this name is connected to the parameter's values. This serves as an easy way to keep track of progress when many simulations have been done.

The model being used is divided into two processes. First process is the design strategy of Carrel [2] for a planar LPDA and second process is to extend it to the non-planar model of Dubrovka [4]. The planar LPDA will only be described briefly here as this has been covered in Chapter 2. It will be expanded to the non-planar case with the apex angle (γ).

3.5.1 Parameters for this LPDA

The relevant parameters for the parameter study of the planar LPDA will now be discussed. The bandwidth was chosen to be four to one (4:1) and with frequency scaling this could be shifted in frequency to any frequency. It was proposed to use the 600 MHz to 2.4 GHz band as this is a part of which the SKA is interested in.

With one LPDA designed fully, one takes a mirror image of it to produce the second

LPDA. These two LPDA's are now placed apart from each other by the apex angle γ

$$\gamma = 2\alpha \tag{3.5}$$

The apex angle is one of the critical parameters which is adjusted in simulation to observe its effects on the antenna's characteristics. The other critical parameter is τ which is also adjusted to see its effect. Table 3.3 shows the value range used for the adjustments in these two critical parameters.

Table 3.3: Parameter sweep value range for α and τ.

Parameter	Value range
α	6° to 30°
τ	0.895 to 0.963

This parameter range was chosen with some practical limitations in mind. At α angles smaller than 6° the two LPDA antennas are almost parallel to each other with an impractically long feed line which is unwanted. At angles larger than 30° the front-to-back ratio (F/B ratio) declines quite rapidly as seen when Figure 3.5 and 3.6 are combined and this is unwanted as we require a directional beam. Discrete steps of 2° were taken as this provided reasonable resolution along with acceptable simulation run-time.

The parameter τ was chosen while having in mind the number of dipoles for each simulation. The number of dipoles is directly related to the value of τ (when τ increases, the number of dipoles also increases) with τ having a maximum of one. The number of dipoles is chosen to be 20 to 60 with increments of 5 each time and this results in the following values for τ: 0.895, 0.915, 0.928, 0.938, 0.945, 0.951, 0.956, 0.960, and 0.963.

The E- and H-plane 3 dB beamwidths are not equal and this is expected as shown in Figure 2.13. To compensate for this oval shape of the beam, the angle γ is slightly decreased in order to produce a more rounded beam. This has been done experimentally and incorporated in this parameter study.

The last parameter that needs to be specified is the number of frequency points that are needed. FEKO uses a frequency solver as mentioned earlier and this will directly affect the simulation run-time. The frequency response was oversampled at first in order to determine the Nyquist rate and then I decided to use double the Nyquist rate which resulted in about 40 frequency points needed per simulation.

3.5.2 Model's code in EDITFEKO

The whole model is coded in EDITFEKO. Some simulation choices are available in order to reduce run-time of each simulation for the parameter study.

3.5.2.1 Simulation choices

One way of reducing run-time is by only simulating one part of the antenna and then combining the second antenna's radiation pattern with the first one. The model consists out of 2 LPDA antennas which are separated by the angle γ. One option is to simulate only one antenna and then duplicate the results in order to obtain the combined result of the pair. This option is compared to the combined structure where both antenna parts are simulated and the results are shown in Figure 3.4. By simulating only half of the structure we gain a faster simulation run-time. The frequency scaling for this surface structure is of the order 6 as described earlier, which means if half the segments are simulated it will result in a simulation run-time that is up to 64 times faster. Computationally this turns hours into minutes and minutes into seconds which is a great advantage. This does not take into consideration the coupling that occurs between the two parts of this antenna. We simulate and compare these two different models to see if this has a major effect on the radiation pattern.

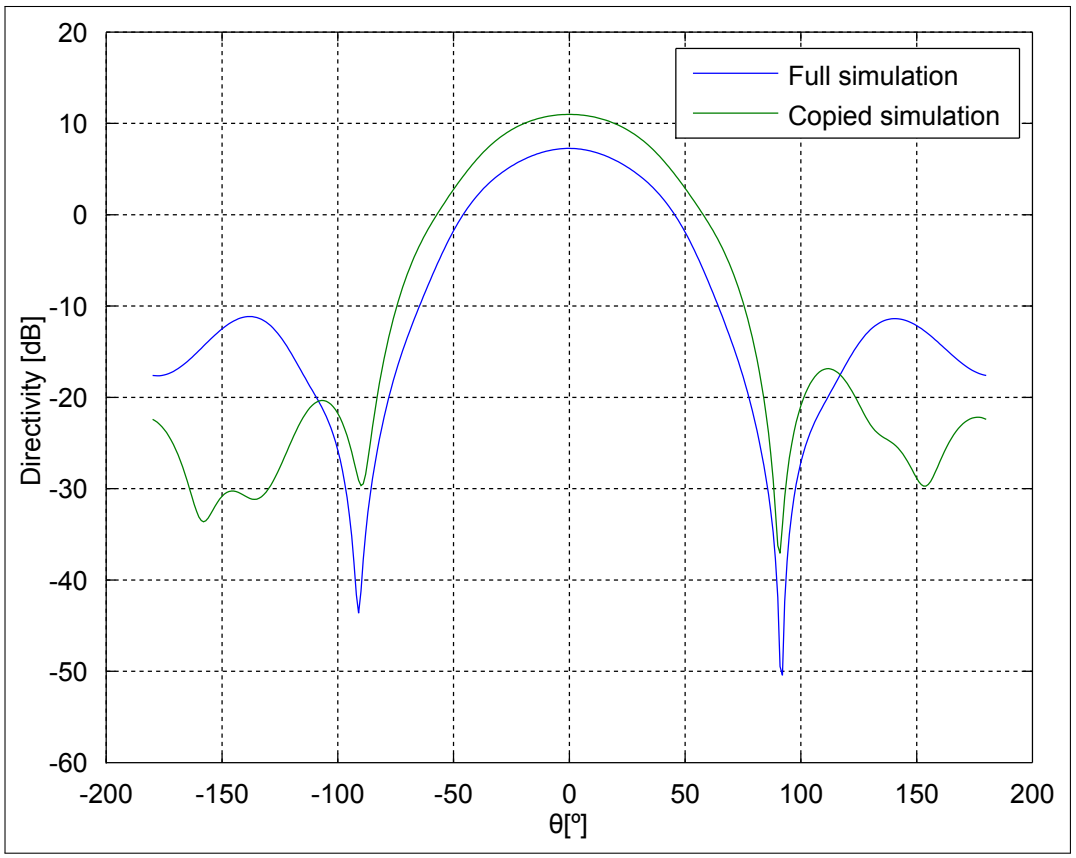

Figure 3.4: Radiation pattern comparison between a model with 2 LPDA antennas and a model with 1 LPDA antenna who's radiation pattern is combined with itself to form a 2 LPDA antenna.

Figure 3.4 shows a difference for the main lobe of 3.7 dB and and a different back lobe shape. This shows that the two parts of the antenna influence each other and cannot

be simulated separately and still produce accurate results. This means that the whole structure needs to be simulated. This was somewhat expected as the antennas are placed closely together.

3.5.2.2 Segmentation choices

Segment sizes are also of interest, especially for the computer that needs to simulate it. The amount of segments would directly affect the simulation runtime. Lesser elements (this would also mean larger elements) present in the model would result in faster simulations. Too few elements again would resolve in inaccurate results and the response would diverge. We do this by making the segments smaller till the results converge.

Furthermore, the shorter elements are meshed finer than longer elements as this is where the high frequency active region is and the long elements are where the low frequency active region is. Testing this mesh refinement showed similar results to the unrefined mesh resulting in the reason for this choice.

3.5.3 Final structure

One simulates the final structure of the antenna by performing a parameter sweep of the critical parameters τ and α. Design curves will be produced and discussed from these simulations in the next section.

3.6 Characterising of Design Curves

Here we show and discuss the relevant results obtained from the simulations in the design curves. The simulations are done as have been previously described and the results shown. The characteristics are explained and the results given in the various figures.

3.6.1 Directivity

The directivity is shown in Figure 3.5 and it is clear that the directivity is mainly dependent on the parameter α and not dependent on τ. At low values of τ too few elements are present to ensure a flat frequency response and a large ripple is present. We are looking for a flat frequency response and thus a ripple that is as small as possible.

Figure 3.5 shows there is a direct relationship between directivity and α. When we increase α, the directivity decrease and when we decrease α, the directivity increase.

3.6.2 Back lobe

The back lobe is the radiation lobe in the opposite direction of the main lobe. We want the directivity in this direction to be as small as possible. The directivity of the back lobe is shown in Figure 3.6.

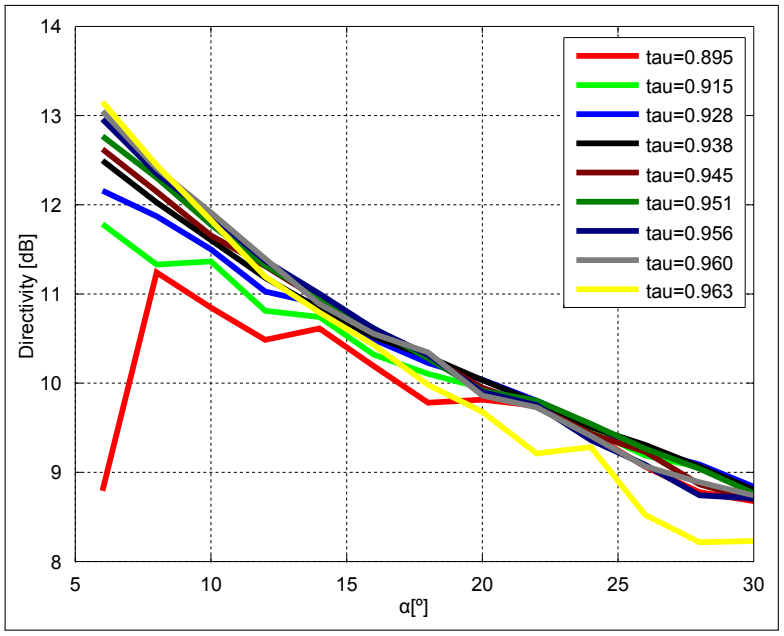

Figure 3.5: Average directivity for a specific τ and α.

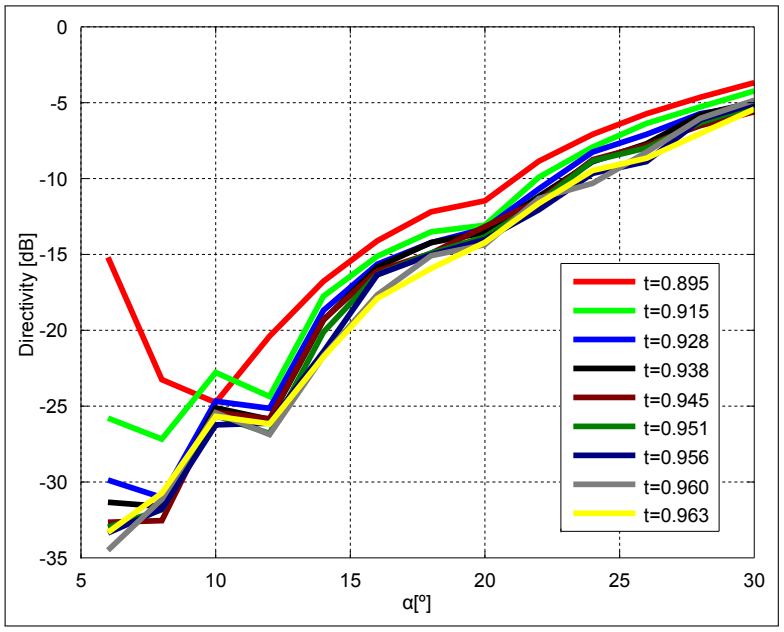

Figure 3.6: Average back lobe for a specific τ and α.

Figure 3.6 shows the back lobe is mainly dependent on α and not dependent on τ. At low values of τ, too few elements are present to ensure a flat frequency response and this results in a large ripple. Very much the similar reasons as for the directivity.

When we increase α, the back lobe also increases and when we decrease α the back lobe decreases. We see a direct correlation between α and the back lobe.

3.6.3 Input Impedance

Figure 3.7 shows the input impedance which can be expected for the antenna. We decided to design for an input impedance of 50Ω as we can easily connect this to measuring equipment with the same impedance. The input impedance is mainly dependent on α and less dependent on τ as we see in Figure 3.7. When we increase α the input impedance decreases and when we decrease α the input impedance increases.

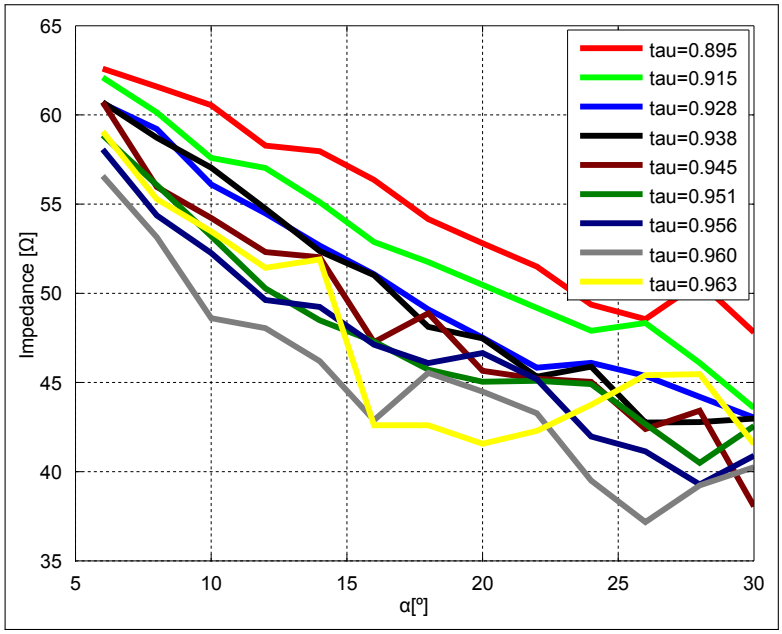

Figure 3.7: Average input impedance for a specific τ and α.

The input impedance is also dependent on the ratio of the feed line width to the thickness of the substrate used. We optimise this ratio to have an impedance of 50Ω to be matched to the system. The input impedance is also expected to vary, within limits, over the frequency band.

3.6.4 Reflection coefficient

The reflection coefficient (S_{11}) is calculated from the input impedance by using Equation 3.6

$$S_{11} = \frac{Z_{in} - Z_0}{Z_{in} + Z_0} \tag{3.6}$$

where the symbols have the following definitions:

S_{11} - The reflection coefficient at the feed point of the antenna.
Z_{in} - The input impedance of the antenna.
Z_0 - The characteristic impedance of the feed line (50Ω) [21].

We further expect the antenna must be matched to a 50 Ω environment. Figure 3.8 shows the S_{11} for the antenna and we calculate this with Equation 3.6. The reflection coefficient must be as low as possible for the received signal to propagate to the rest of the system.

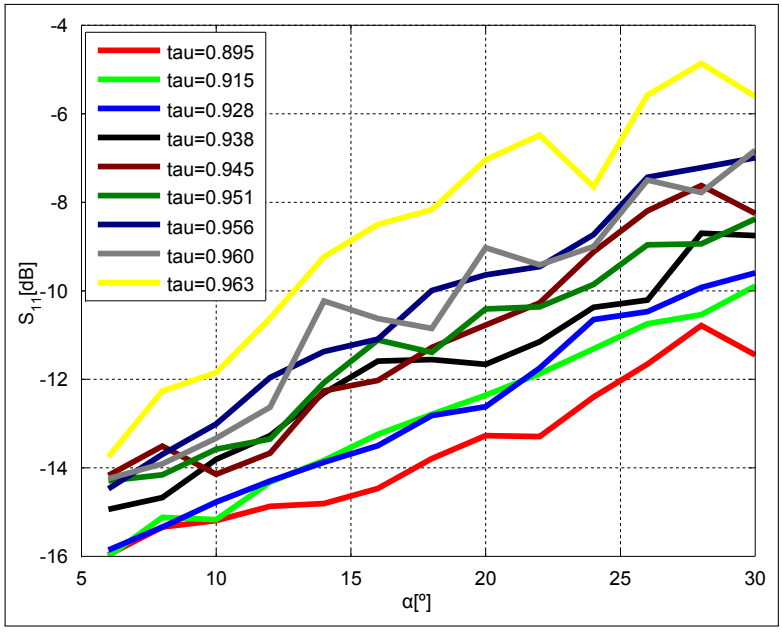

Figure 3.8: Average reflection coefficient for a specific τ and α.

The reflection coefficient shows how much energy is reflected back into the antenna and therefore it must be as small as possible. We see in Figure 3.8 the reflection coefficient is dependent mainly on α and not on τ. When we decrease α, the reflection coefficient decreases and when we increase α, the reflection coefficient increases.

3.6.5 Cross Polarisation

We determine the cross polarisation with Ludwig 3 from [22]. The purity of the cross polarisation is of importance here as this leads to the possibility of having two communication channels in the same bandwidth. This is of significance as the possibility exists to double the effective bandwidth. According to the IEEE the standard definition of cross polarisation is "*The polarization* (polarisation) *orthogonal to a reference polarization* (polarisation)" [23]. We will be working in a rectangular coordinate system and choose one unit vector as the reference polarisation and the other as the cross polarisation.

FEKO calculates the E-field in the spherical coordinate system. We then transform the field to the rectangular coordinate system with Equations 3.7 and 3.8 from Ludwig's third definition of cross polarisation [22].

$$R(\theta,\phi) = E(\theta,\phi)\cdot[\sin\phi\underline{\mathbf{i}}_\theta + \cos\phi\underline{\mathbf{i}}_\phi] \tag{3.7}$$

$$C(\theta,\phi) = E(\theta,\phi) \cdot [\cos\phi \underline{\mathbf{i}}_\theta - \sin\phi \underline{\mathbf{i}}_\phi] \tag{3.8}$$

Here $R(\theta,\phi)$ represents the co-polarisation (also called the reference polarisation) and $C(\theta,\phi)$ the cross polarisation. The E-field is shown in Figure 3.9 on a flat plane. The E-field radiates from the antenna in the y-direction and we choose this as the co-polarisation. We normalise all the fields with reference to the field at the origin. Every point in the plane has an E-field component in the x- and y-direction. With the y-component being the reference, the x-component is the cross polarisation. The x-components size increases as we move further away from the two axis [1]. We take a worst case scenario and calculate the cross polarisation at a 45° angle, with reference to the x-axis. We calculate the cross polarisation (CP, Equation 3.9) by using Equations 3.7 and 3.8.

$$CP = \frac{R}{C} \tag{3.9}$$

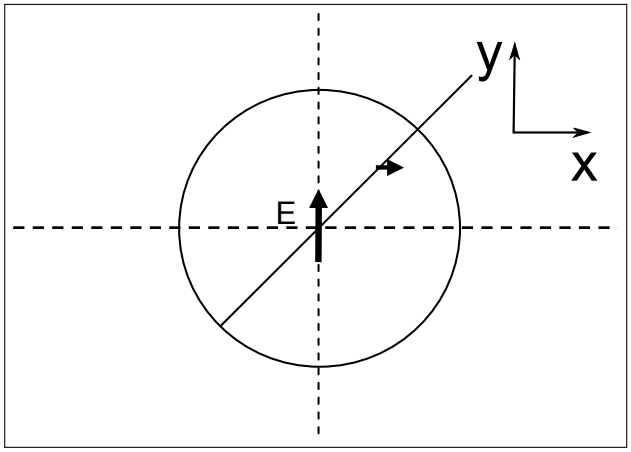

Figure 3.9: Cross polarisation pattern.

We calculate the cross polarisation for the non-planar LPDA and show the results in Figure 3.10. We see here the cross polarisation is mainly dependent on α and not dependent on τ. At low values of τ the amount of dipoles are too few to ensure a flat frequency response. As we decrease α, the cross polarisation decreases and as we increase α, the cross polarisation increases.

3.6.6 Beamwidth

The term beamwidth refers to the -3 dB beamwidth. This is the angle that forms between the two points that are 3 dB smaller than the maximum of the radiation pattern [1].

The -3 dB and -10 dB beamwidths are dependent on α and not dependent on τ as in Figures 3.11 and 3.12. The value of τ needs to be high enough to result in a flat frequency

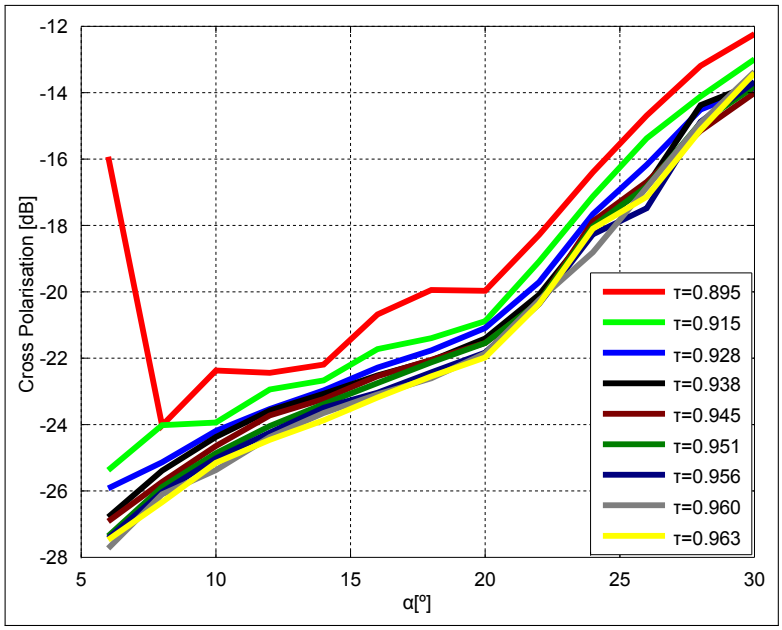

Figure 3.10: Average cross polarisation for a specific τ and α.

response. At low values of τ too few elements are present to ensure a flat frequency response.

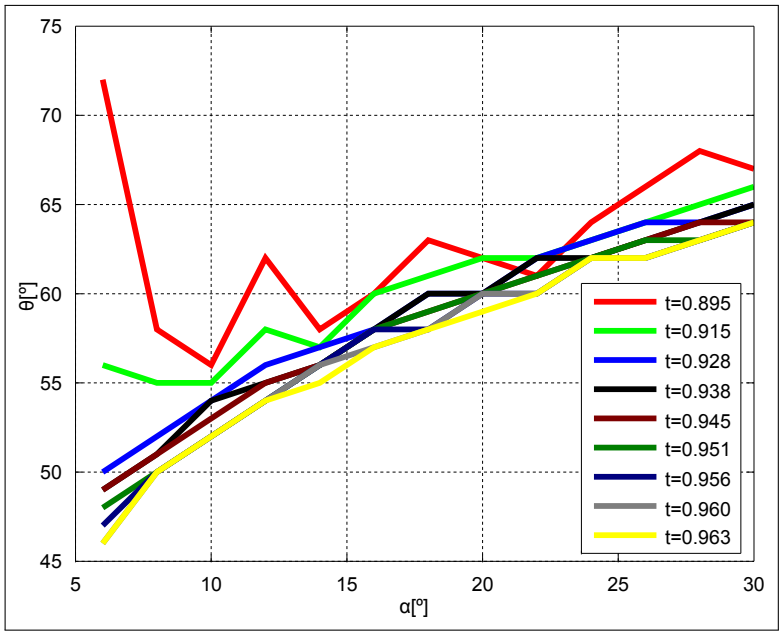

Figure 3.11: Average half power beamwidth for a specific τ and α.

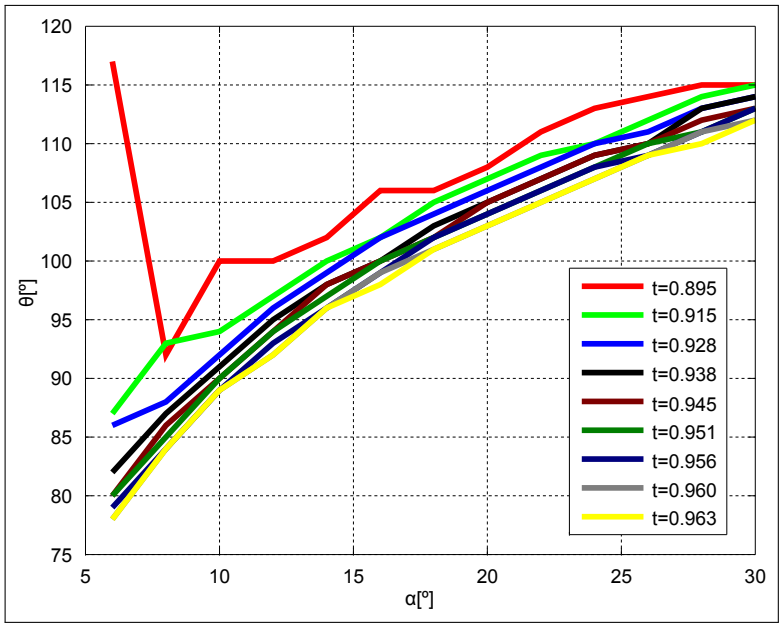

Figure 3.12: Average -10dB beamwidth for a specific τ and α.

3.6.7 Roundness of radiation pattern

This antenna was first designed to operate in a reflector dish environment, but later decided to use as a direct radiating element, thus showing the interest in the roundness of the pattern. We see the roundness of the pattern in Figure 3.13. This shows us how circular the radiation pattern is as opposed to oval shaped. A round (or circular) radiation pattern is needed if to be used as a feed for a round dish. The radiation pattern for this type of antenna is unfortunately oval-shaped (the E- and H-plane electric fields are not equal) and we need a round pattern to illuminate a dish effectively and minimise spillover. Spillover is the part of the main beam that does not fall on the dish, but on the ground (or space).

Figure 3.13 shows the oval shape of the radiation pattern. We take two pattern cuts, one x-axis (E-plane) cut and one y-axis (H-plane) cut and compare the two with each other. These two cuts are thus orthogonal on each other. The angle Δ determines the difference in beamwidth of these two cuts. If the Δ angle is 6°, it means the y-axis's beamwidth is 6° larger than the x-axis's beamwidth. This gives us an indication of the roundness of the radiation pattern. A Δ angle of 0° means the pattern is round.

We do not see a clear pattern emerging from Figure 3.13. This is because we have optimised the simulation for a round radiation pattern at -3 dB. In the figure we see all the Δ angles are small and thus preferred for a dish environment.

When we look at the -10 dB pattern roundness a pattern does emerge. In Figure 3.14 we see that the Δ angle is dependent on α and not dependent on τ. Again we see that at

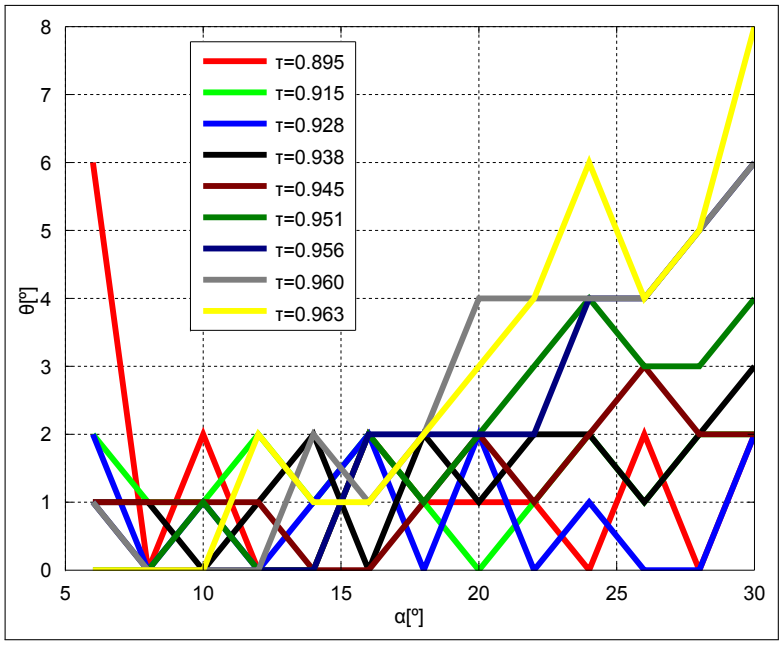

Figure 3.13: Average -3 dB pattern roundness for a specific τ and α.

low values of τ, few elements, the pattern roundness is unpredictable due to a non-flat frequency response. When we increase α, the pattern becomes more oval and when we decrease α, the pattern becomes more round.

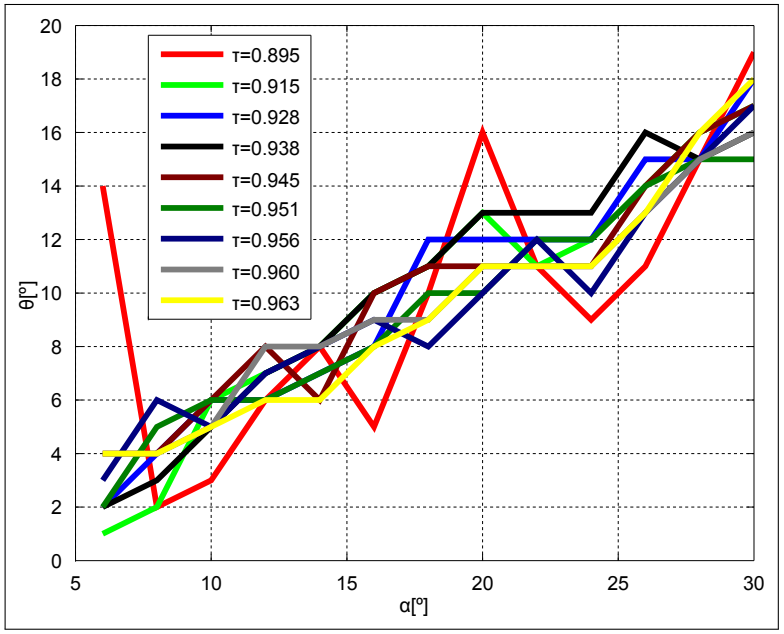

Figure 3.14: Average -10 dB pattern roundness for a specific τ and α.

3.7 Design example using the design curves

We test these design curves by doing a simple design using these design curves. We do this to show the design strategy is accurate and serves as verification for the data generated.

We pick a certain specification and then follow the design procedures. The specific τ and α values are derived from the specifications and we use the generated figures to estimate the performance of the antenna. We simulate the specific model and compare the results with the estimated values.

3.7.1 Design Specifications

Let's assume the specifications for an LPDA antenna is as follows:

- -10 dB at 50° beamwidth

This means that the gain must be 10 dB smaller at $\theta = 50°$ than at $\theta = 0°$.

3.7.2 Solution

We first determine the cone beam. The cone beam is double the beamwidth and is 100°.

We consult Figure 3.12 and find the point where the line crosses the 100° line. The dark green ($\alpha = 16°$) and brown ($\alpha = 14°$) cuts this line. We also prefer a higher τ value as this gives a flatter frequency response.

We choose $\alpha = 16°$ and $\tau = 0.945$ and the other parameters we get from the respective figures as listed below.

- Figure 3.5 shows an average gain of 10.6 dB can be expected.
- Figure 3.6 shows an average back lobe of -16.1 dB can be expected.
- Figure 3.7 shows an input impedance of 47.3 Ω can be expected.
- Figure 3.8 shows an S_{11} of -12 dB can be expected.
- Figure 3.9 shows a cross polarisation of -22.5 dB can be expected.
- Figure 3.14 shows the pattern roundness is 10°.

3.7.3 Results

The simulated results of the design example follows. Only the results that are considered important are shown here.

3.7.3.1 Roundness of pattern

In Figures 3.15, 3.16 and 3.17 we see the pattern roundness. Each time we cut at a specific frequency. The cuts are at $\phi = 0°, 30°, 60°, 90°, 120°$, and $150°$. We sample the frequencies at the bottom, middle and top of the frequency band. From the figures we see that the pattern is round in the main beam.

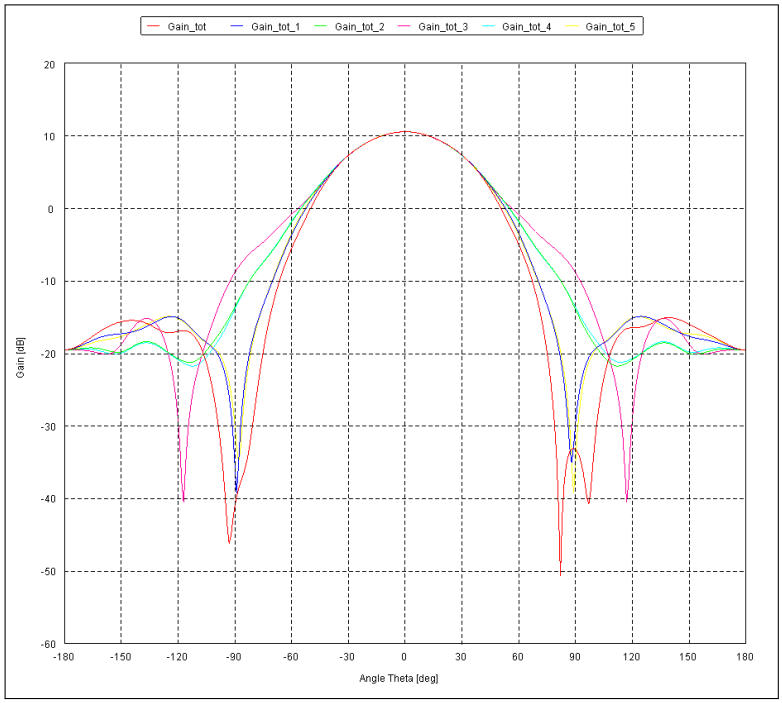

Figure 3.15: Gain at 1.5 GHz.

3.7.3.2 Gain

Figure 3.18 shows the gain over the frequency band. The gain is very stable over the band, which means the whole band is covered, thus the bandwidth is very large as specified. The average gain closely resembles the predicted gain of 10.6 dB.

3.7.3.3 Cross Polarisation

Figure 3.19 shows the cross-polarisation over the frequency band. It varies very little over the band and is quite close to the predicted value for the cross-polarisation of -22.5 dB.

3.7.3.4 Back lobe

Figure 3.20 shows the back lobe of the radiation pattern. We see that it correlates well with the predicted value of -16.1 dB. It is also constant over the whole band.

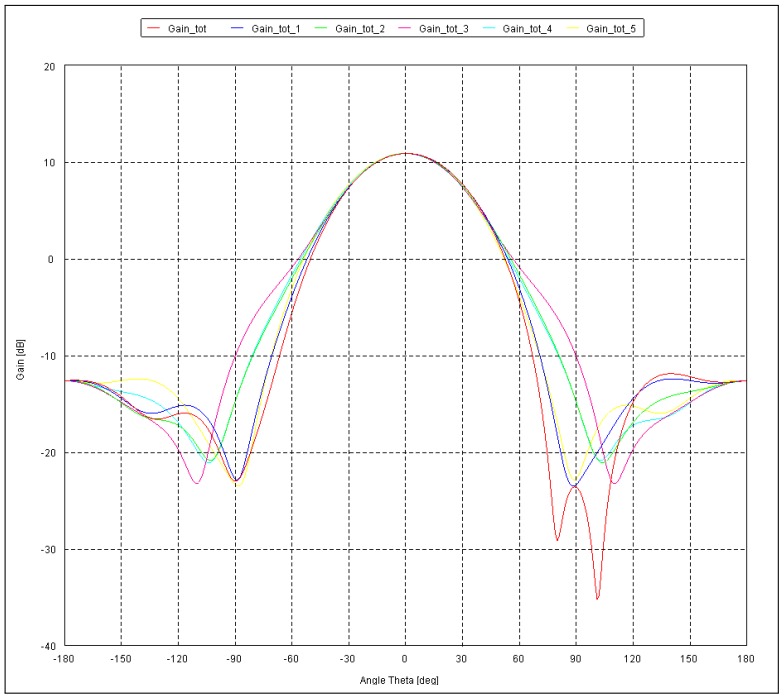

Figure 3.16: Gain at 600 MHz.

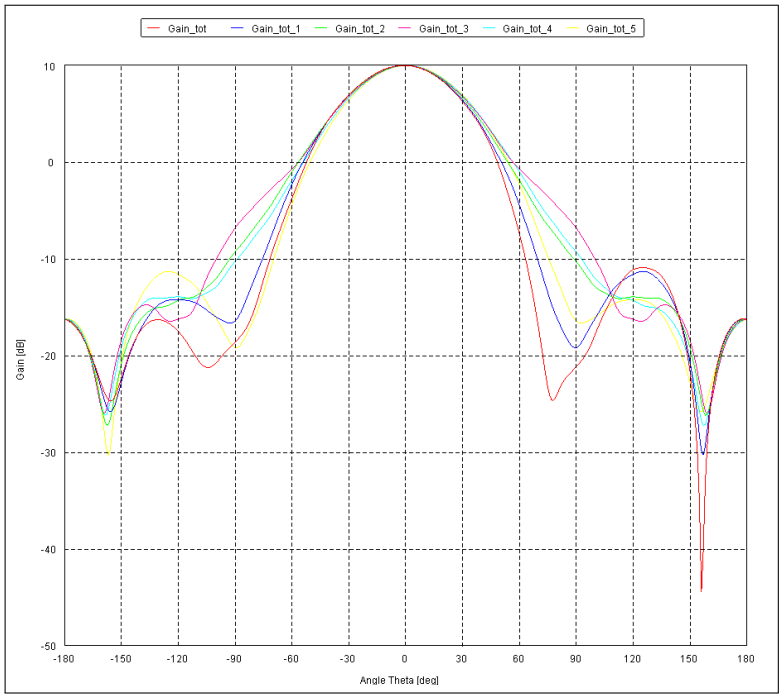

Figure 3.17: Gain at 2.4 GHz.

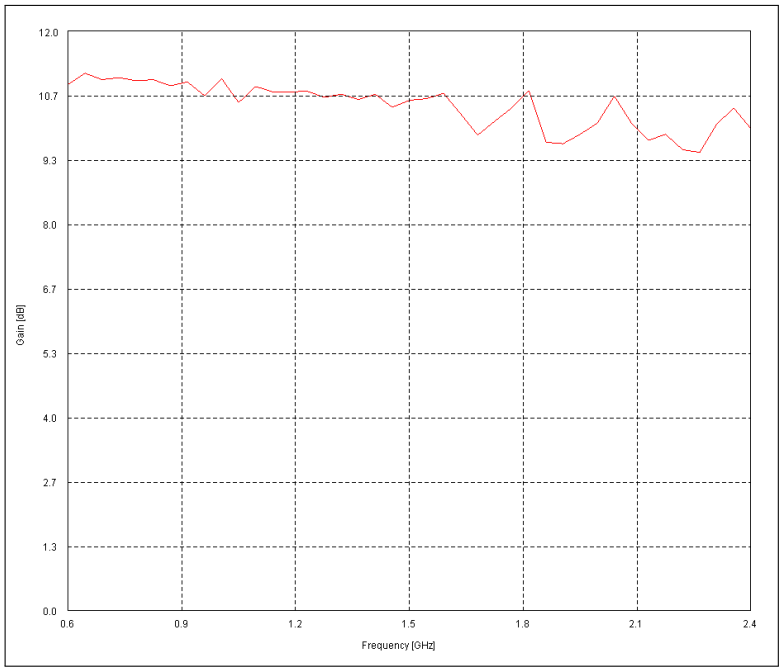

Figure 3.18: Gain across the frequency band.

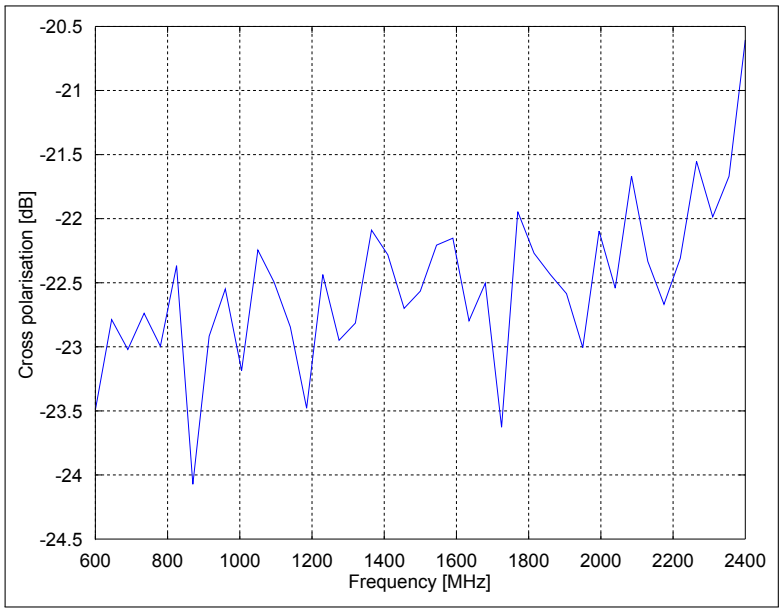

Figure 3.19: Cross polarisation over the frequency band

3.7.3.5 Reflection coefficient

Figure 3.21 shows the reflection coefficient across the band. It correlates well with the predicted value of -12 dB.

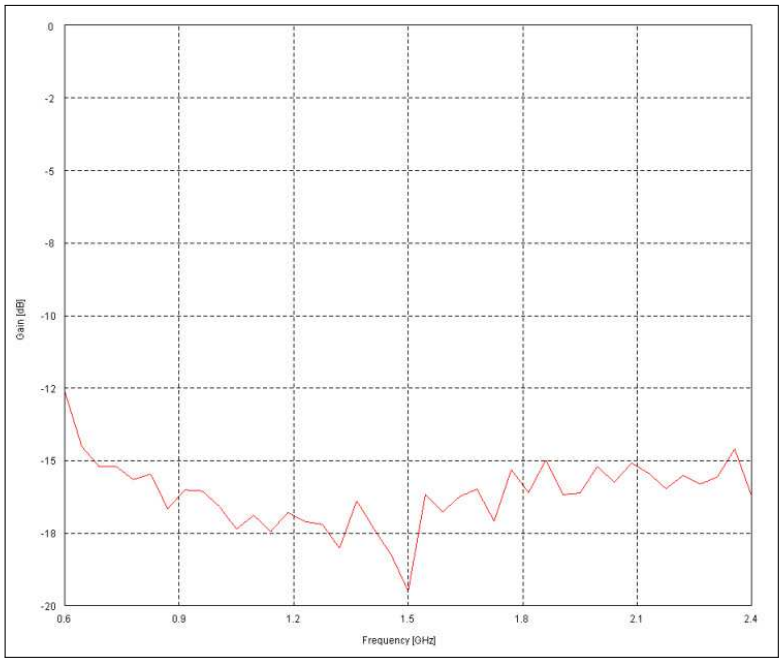

Figure 3.20: Back lobe across the frequency band.

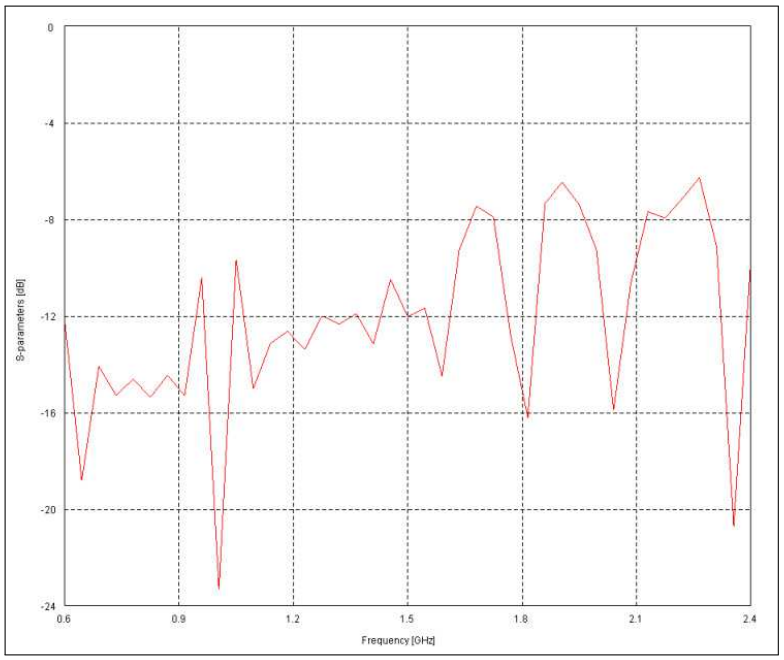

Figure 3.21: Reflection coefficient across the frequency band.

3.7.3.6 Beamwidth

Figure 3.22 shows the gain across the ϕ-angle at the center frequency of 1.5 GHz. The red graph shows us the maximum gain and the blue graph the gain at $\phi = 50°$. This means the cone beam is 100°. The blue graph is about 10 dB less than the maximum. This means

the gain at angle $\theta = 50°$ is 10 dB smaller than the gain at angle $\theta = 0°$. We expect this result as it is the specification received. Figures 3.23 and 3.24 shows the beamwidths for the 600 MHz and 2.4 GHz frequencies respectively.

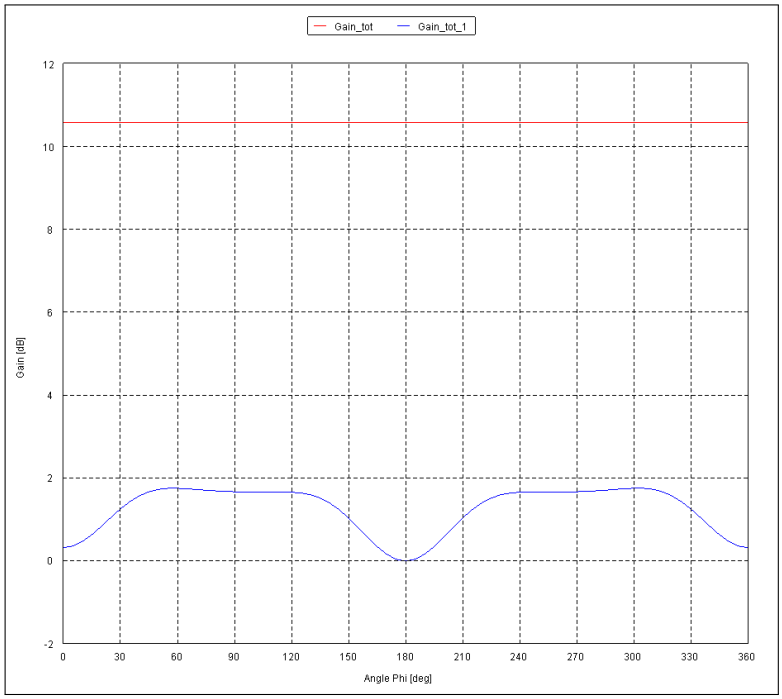

Figure 3.22: Gain for ϕ angle at 1.5 GHz.

The gain of the two figures above is about 10 dB less than the maximum gain. We take these measurements at $\phi = 50°$ as well. It correlates with what we expect from design example. This means the gain is about 10 dB less at $\theta = 50°$ than at $\theta = 0°$.

To summarise, we have shown that the design curves created can be used to design an LPDA antenna. We move on to building a scale model and measuring in the following sections.

3.8 Scale model LPDA manufacturing

To further test the design procedure (other than through simulation) we build a scale model with 1.5-6 GHz bandwidth. Figure 3.25 shows the complete structure that is about 160 mm high with a base of 100 mm by 100 mm. We opted for a dual polarised antenna model as it is rather little extra work and would provide both polarisations. The cross polarisations is quite low (below -20 dB) and should not influence the other polarisation.

FR-4 is the dielectric substrate used in the fabrication of the scale model. FR-4 was chosen

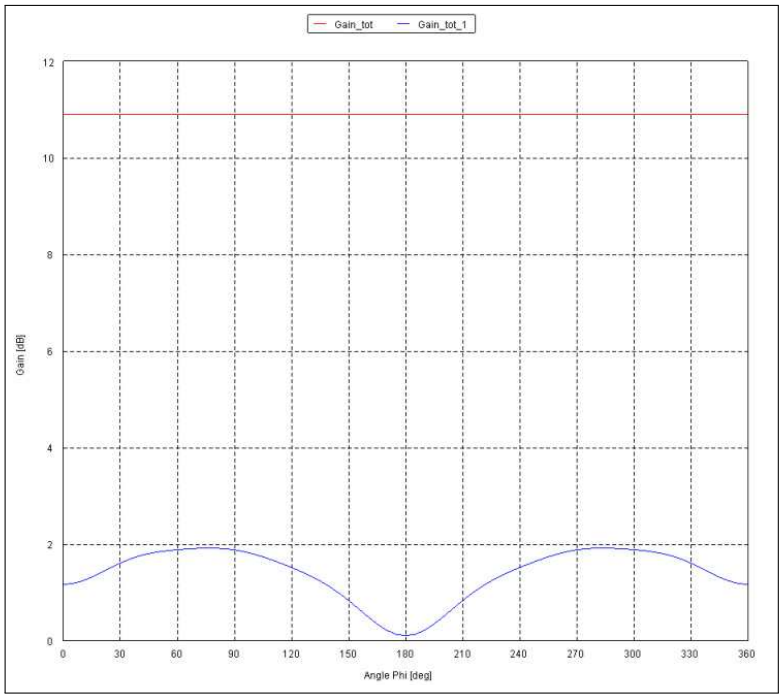

Figure 3.23: Gain for ϕ angle at 600 MHz.

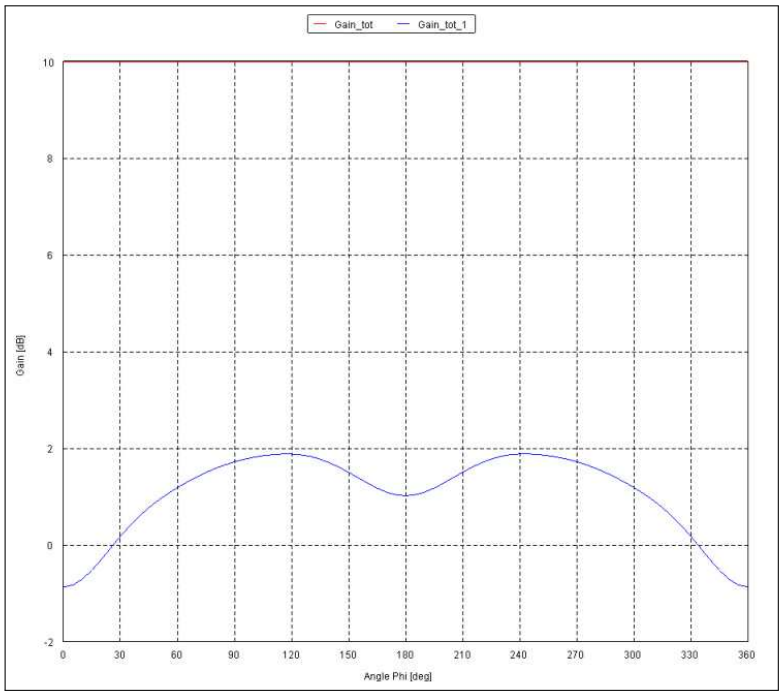

Figure 3.24: Gain for ϕ angle at 2.4 GHz.

as it is inexpensive and can be used for printed circuit boards (PCB's) as well as for antennas. The relative permittivity of FR-4 is 4.33 and the loss tangent is 0.02 as measured by Djordjevìc et al. [24].

Figure 3.25: Manufactured dual polarised LPDA antenna printed on FR4 PCB.

The antenna designs were given to Mr. Wessel Croukamp for manufacturing. This entails putting a mask of the antenna on an FR-4 dielectric that is coated with copper. We choose a 1.6 mm thick dielectric as this reduces the offset of the dipoles on either side of the board and is still thick enough to not break easily. Then it is submerged in an acid solution that removes the unwanted copper from the substrate. The boards are cut to size and a 50 Ω coaxial line is soldered onto the antenna. The outer conductor is connected to the one side of the board, while the center conductor is extended and soldered onto the other side of the board. This process forms one part of the final structure that consists of four parts. All four parts might look exactly the same, but only two parts are, the other two parts are mirror images of the first two. The pyramidal structure is placed on a foam pedestal as shown in Figure 3.25 in order to handle the structure easily. The electrical characteristics of the foam are very close to air and thus should not influence the antenna's performance.

3.9 Measured results

Here we are mainly interested in the radiation pattern of this antenna. Seeing as two of the antennas work together we connect the two coaxial line conductors to form one port. Both antenna parts have normalised impedances of 50 Ω and when they are connected in parallel they form 25 Ω. This is however a problem as the measuring equipment available are 50 Ω and we do not have an impedance transformer. Thus we will only measure and comment on the radiation pattern of this scale model.

Unfortunately for the dual polarised model, the measured results did not correlate with the simulated results. This is due to manufacturing tolerances, the circuit board properties and the assembly of the four parts of the antenna. Some dipoles actually touched dipoles of the adjacent board and deformed the radiation pattern. It was decided to remove the second polarisation and only measure the one polarisation. Figure 3.26 shows the measured half power beamwidth compared to the simulated half power beamwidth for the single polarisation scale model.

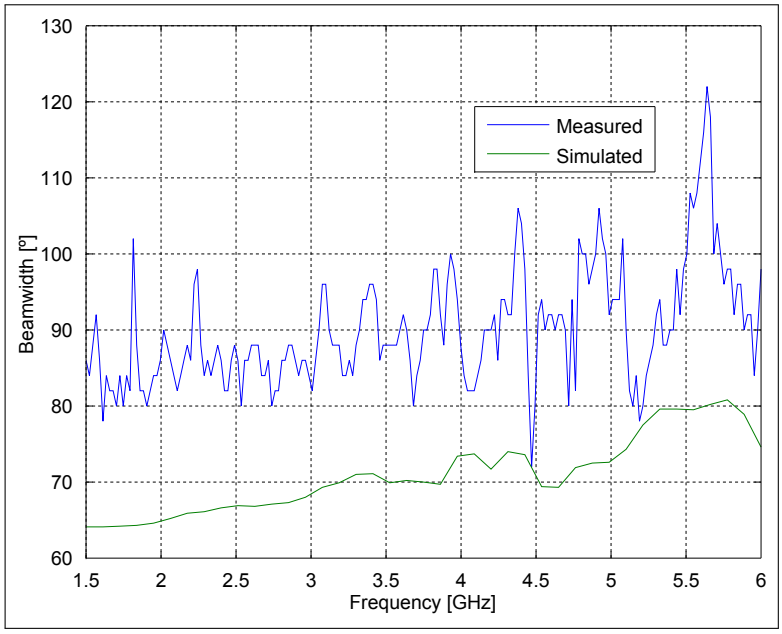

Figure 3.26: Measured half power beamwidth radiation pattern compared to simulated half power beamwidth radiation pattern for the single polarised scale model.

Figures 3.26 shows that the simulated and measured results do not look similar with an average difference of about 20°.

3.10 Conclusion

The LPDA's properties can be determined experimentally, as shown in the figures. In all circumstances it is required that the value of τ must be kept large enough as this parameter determines directly the number of dipoles present and ensures s flat frequency response. If τ is chosen too low, the ripple in the frequency becomes too high.

All the properties in this report is mainly dependent on α. These properties are the directionality, back lobe, input impedance, reflection coefficient, cross polarisation, beamwidth and pattern roundness.

From Figures 3.15, 3.16 and 3.17 we see the radiation pattern is round. The bandwidth is

also ultra wide with a 4 : 1 relationship, thus the project specification is achieved.

We characterised the non-planar LPDA according to his parameters. We can also predict certain results when we get certain specifications. This means the design strategy is a success for the non-planar LPDA.

Unfortunately the measured results did not compare well with the simulated results.

This chapter was for a high performance antenna, next we look at a low-cost antenna.

3.11 Recap

In this chapter the following was discussed:

1. the design of an LPDA antenna
2. FEKO is choice of simulation package with MoM technique
3. parameter study through simulation
4. antenna characteristics plotted and discussed
5. manufacturing of an LPDA antenna on PCB
6. measurements and discussion of measured antenna

Chapter 4

Zig-Zag Antenna Design

4.1 Introduction

As stated in Chapter 2 log-periodic antennas were introduced by DuHamel [12] and he showed that a wire outline of the antenna produced similar results to a planar antenna. Having this in mind we can simplify the wire log-periodic antenna in Figure 2.8 to a triangular tooth or "Zig-Zag" antenna as proposed by DuHamel [14]. Figure 4.1 shows the zig-zag structure and it is quite similar to the trapezoidal tooth structure.

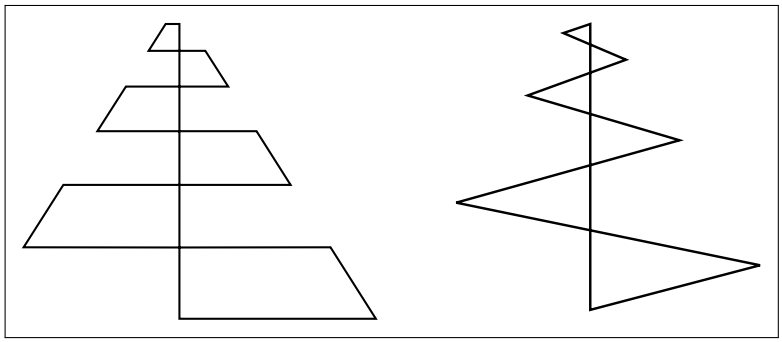

Figure 4.1: A trapezoidal tooth structure (left) and a zig-zag structure (right).

This antenna structure is expected to be very cheap to manufacture and a possibility for the SKA. The idea is to have a jig or frame and then someone bend a wire according to this. This should be very quick and easy to do, but problems could arise as several thousand are required.

This chapter follows a similar trend to the previous one where we do a parameter study and generate design curves. We build a prototype antenna and measure it to compare with simulation. The measured results showed much interference from the environment and we suggest using a better measuring site.

4.2 Parameter study

For the zig-zag antenna we use a similar model as the LPDA in Chapter 3, with the difference of using triangular wires as to rectangular surfaces. We obtain design curves by performing a parameter sweep of the characteristic parameters of the zig-zag and discuss the relevant results.

4.2.1 Front to back ratio

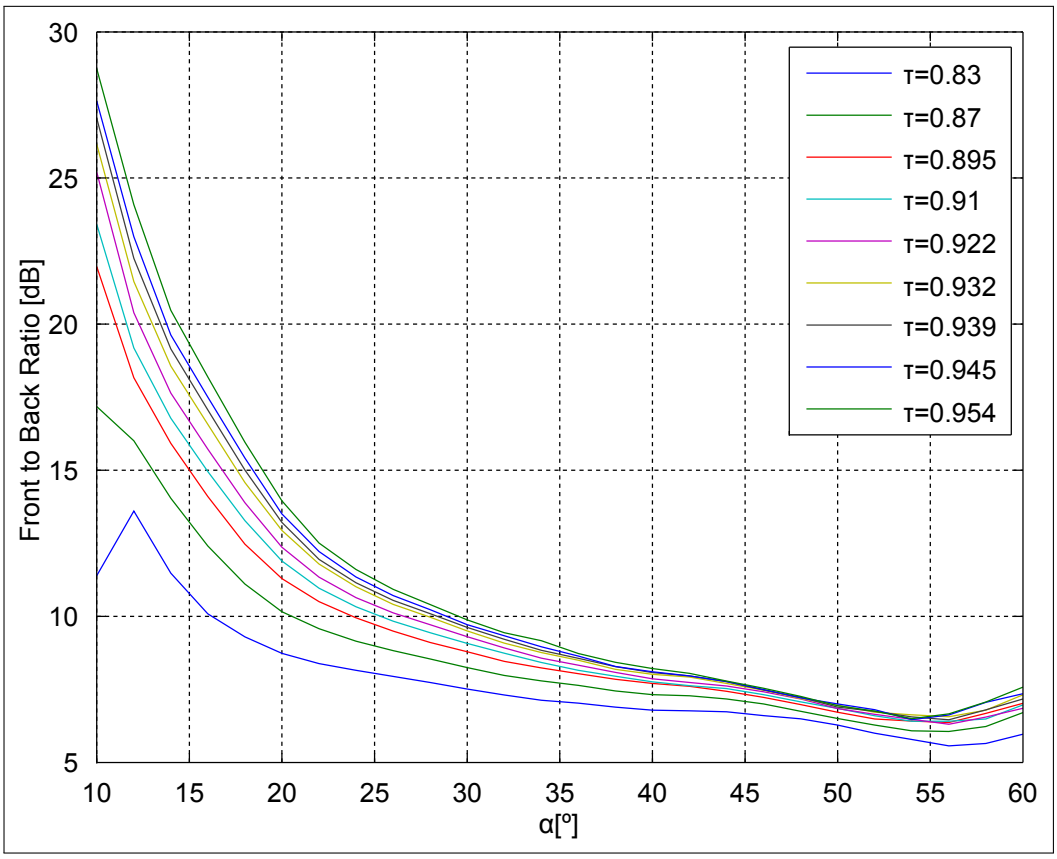

Figure 4.2: Average front to back ratio for a specific τ and α.

The front to back ratio is shown in Figure 4.2 and it is clear that it is mainly dependent on α and to a lesser extend dependent on τ. If low values of τ (τ below 0.87) are combined with low values of α (α below 15°) the elements are too few and far spaced apart to ensure a flat frequency response and we observe the result diverges from the expected result.

When we increase α the front to back ratio decreases meaning that the main lobe becomes smaller and the back lobe larger. When we decrease α the front to back ratio increases. There is however a limit for this, when α becomes very small (less than 15°) the antenna height becomes an issue and some careful thought needs to be taken here. With high

values of α (above 50°) the spaces between the elements become quite small and the wire thickness plays a part here and for the dual polarised antenna the dipoles of the two polarisations would touch which is unwanted. We would suggest using values for α that are between 15° and 45° and τ between 0.895 and 0.954 which relates to 15 to 60 number of elements.

4.2.2 Directivity

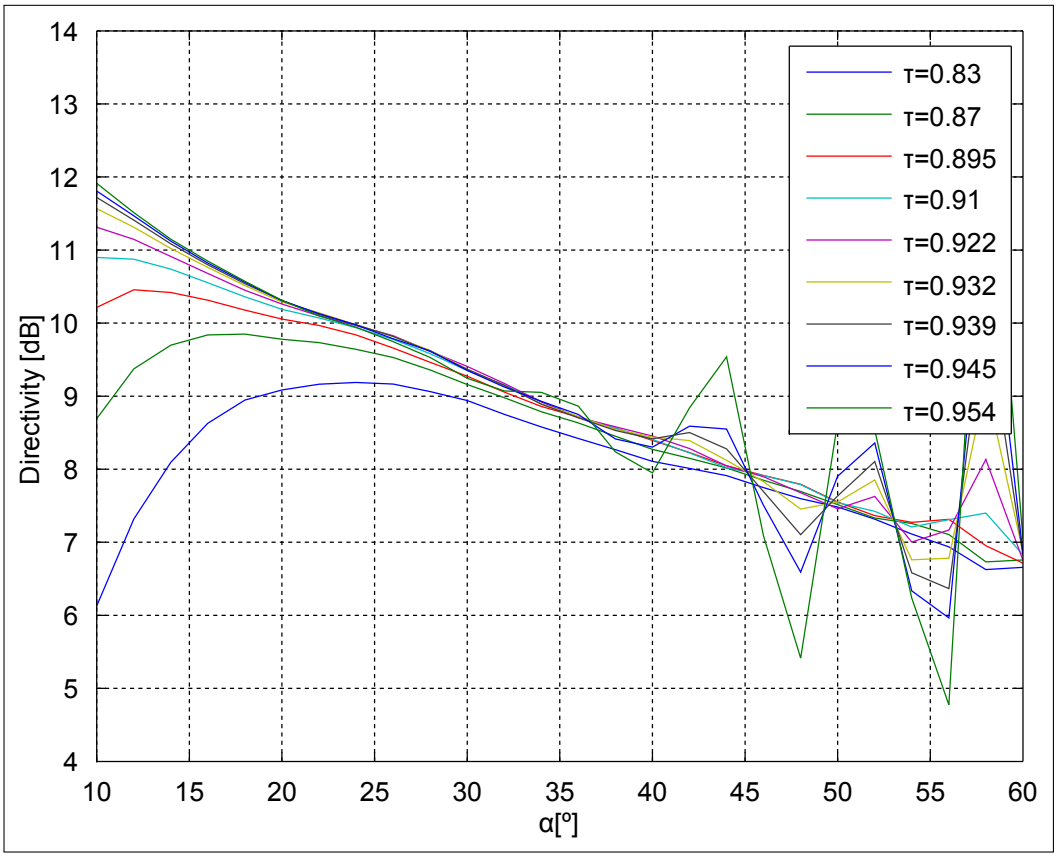

Figure 4.3: Average directivity for a specific τ and α.

Figure 4.3 shows the average directivity to be expected when a certain α and τ are chosen. Here we see a similar response as for the front to back ratio by increasing α the directivity drops and by decreasing α the directivity rises.

4.2.3 Beamwidth

Figure 4.4 shows the half power beamwidth for the E-plane. Here the beamwidth is slightly dependent on α and as α increase so does the beamwidth. The beamwidth does flatten off at $\alpha = 35°$ to about 63°. We expected the increase of beamwidth seeing as the directivity lowers as we increase α.

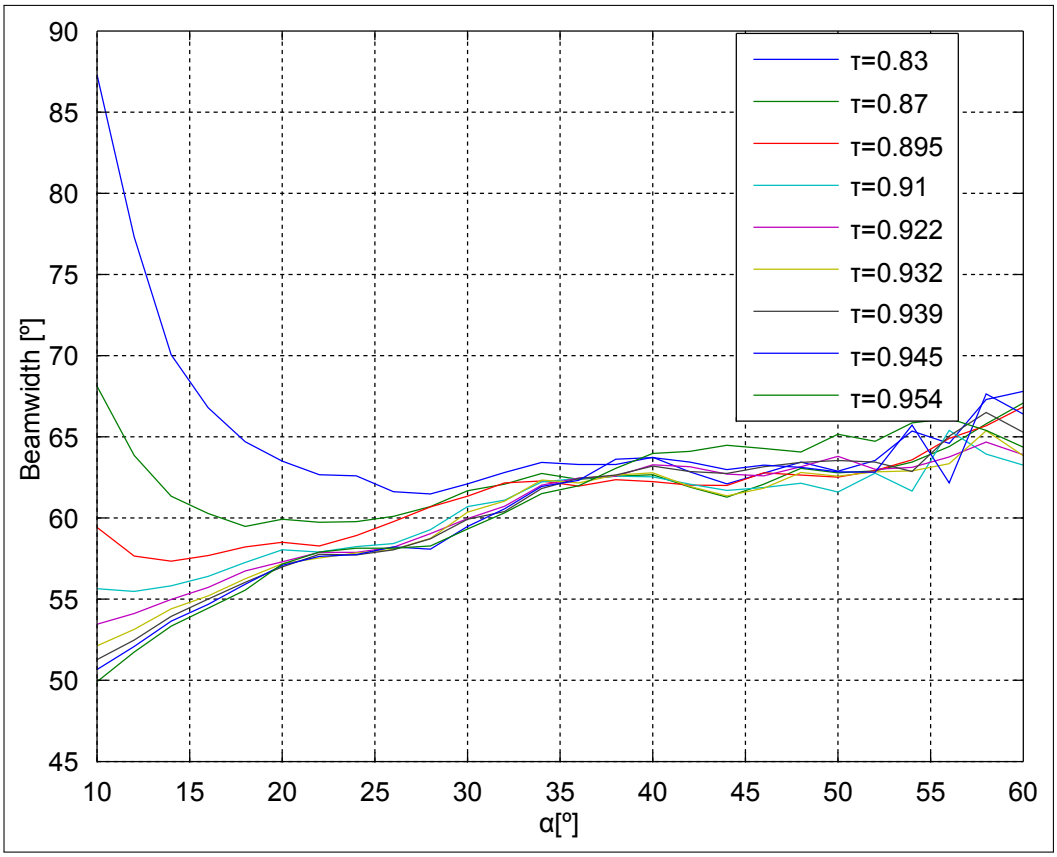

Figure 4.4: Average beamwidth for a specific τ and α.

4.2.4 Input impedance

Figure 4.5 shows the input impedance one can expect for the zig-zag structure. As α is increased the average input impedance decrease and a higher τ produces a lower impedance.

4.2.5 Cross polarisation

Figure 4.6 shows the cross polarisation for the zig-zag structure. Here we observe the cross polarisation to be dependent mainly on α and less dependent on τ. When α increases so does the cross polarisation and when α decreases so does the cross polarisation.

4.3 Design zig-zag antenna

We want to achieve a certain specification and thus we design accordingly. The specifications for the low frequency array are likely to be $\pm 45^\circ$ for the half power beamwidth, dual polarisation, 7:1 bandwidth operating in the 70 - 450 MHz band, and be cheap to manufacture. Figure 4.4 shows the beamwidth can maximally be just above 60° when

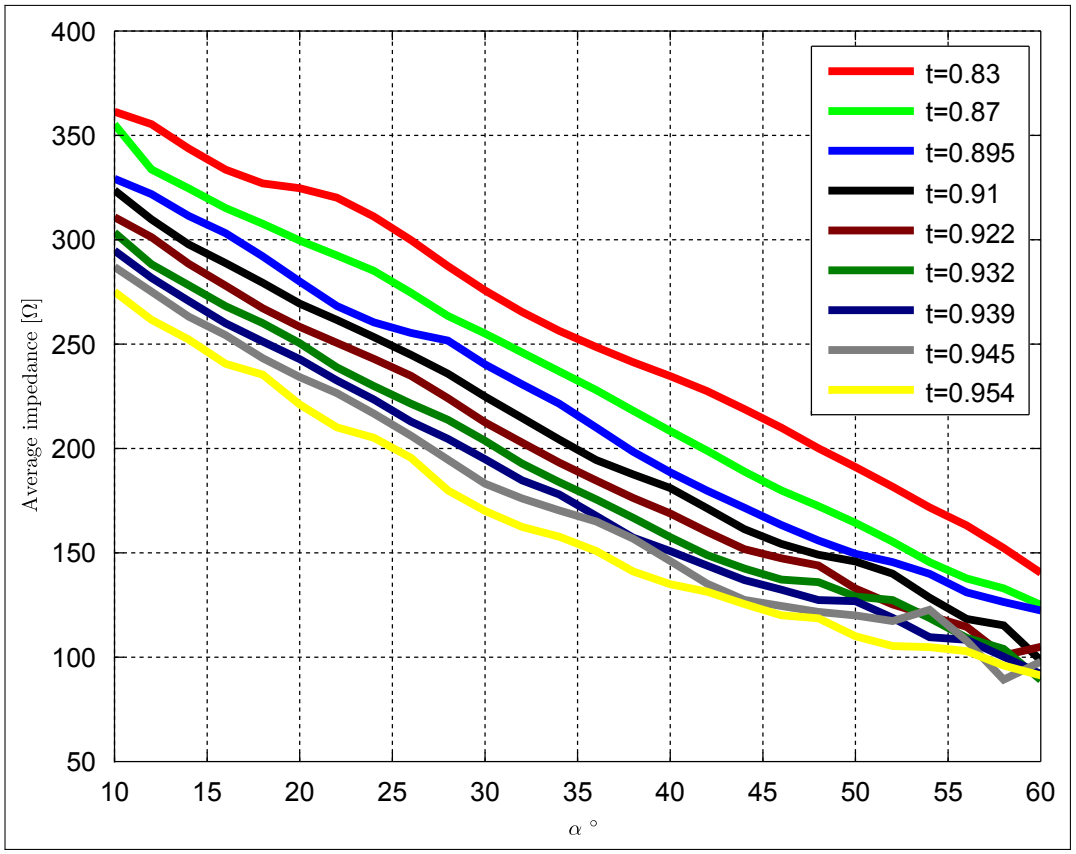

Figure 4.5: Average real input impedance for a specific τ and α.

$\alpha = 40^\circ$ and for higher values the variation in the antenna's frequency response becomes significant and thus we choose $\alpha = 40^\circ$. The design curves are not very sensitive to τ and as a low τ results in fewer dipoles which is likely to lead to cheaper antennas we opt for $\tau = 0.83$.

We have chosen a design and the performance of this design can be estimated from the design curves above with the estimated performance listed below.

- Front to back ratio of about 7 dB.
- Directivity of about 8 dB.
- Beamwidth of about 63°.
- Input impedance of about 230 Ω.
- Cross polarisation of about -6.5 dB.

From the estimated performance we see the beamwidth is only 63°. This is most likely going to be problem as the specification is 90° and we can not reach it. It also seems that there might be a fundamental limit on the beamwidth. In Padhi's [9] report three

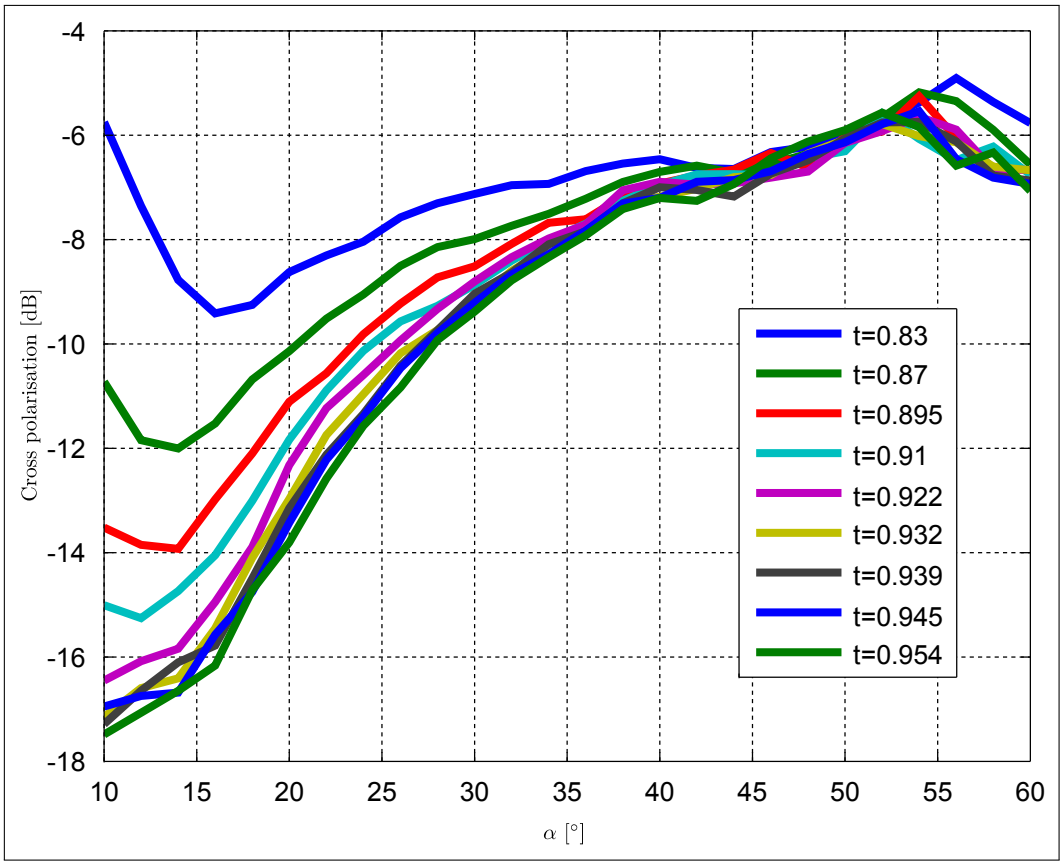

Figure 4.6: Average cross polarisation for a specific τ and α.

antennas are compared to each other as likely candidates for the SKA low frequency array which consists out of spiral, vivaldi and log periodic antennas. These antennas produced half power beamwidths of up to about 70° which suggests a possible limit on the beamwidth.

This antenna is quite large and we suggest a way to make it smaller in the following section.

4.4 Antenna size reduction

For practicality, and for easier handling of the antenna, we limit the footprint of the antenna to 1m^2. There is likely to be a size limitation for the antennas in the SKA low frequency array but we are not yet 100% sure about this. One could argue that at the site there is unlimited space available for large antennas, but large antennas could provide problems in terms of increasing costs, manufacturing and maintenance. The lower frequency (long) dipoles are bent in order to fit into this constraint.

Exactly how much the antenna is affected by bending it we will now find out by simu-

lating the two cases. We will simulate the folded and unfolded antennas and discuss the related results.

We start the folding process by considering one zig-zag arm as shown in Figure 4.7 (Step

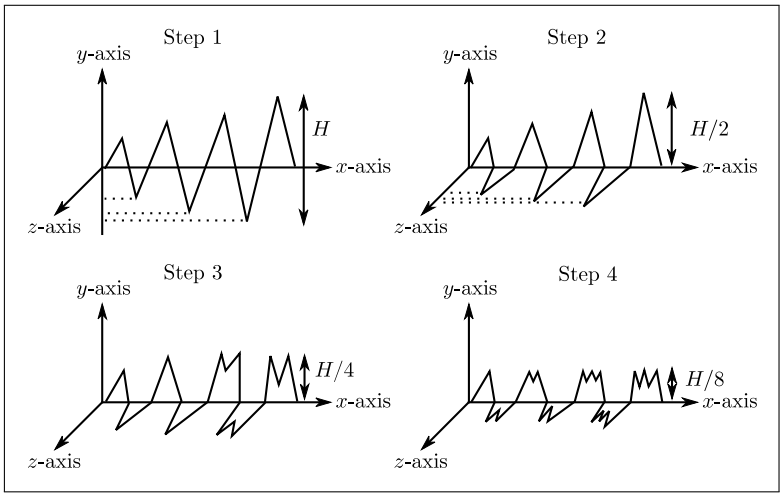

Figure 4.7: Step by step miniaturisation process. Step 1: original height H. Step 2: folded height $H/2$. Step 3: twice-folded height $H/4$. Step 4: thrice-folded and final height of $H/8$. Redrawn from Sharma [5].

1). This structure's height in the y-axis can be defined by H. We first fold the part that is underneath the x-axis by 90° to lie in the xz-plane as shown in (Step 2). Now the height of the structure is $H/2$ and thus half of its original height. Next we fold the longer elements in on themselves as shown in (Step 3). The structure is now $H/4$ high. We can repeat this one last time in order to get to (Step 4) with a structure height of $H/8$. For our structure we omit (Step 1) to accommodate 4 elements.

One would expect the characteristics to change significantly as folding the elements reduces the effective electrical length of each element. By folding only the longest dipoles, one expects the high frequency part of the antennas characteristics to stay the same, but that the low frequency part would be affected.

We now compare two of the same antennas with each other. Both are two arm zig-zag antennas with the same design parameters. The one is unfolded (straight) while the other is folded twice, up to (Step 3) in Figure 4.7. The unfolded structure is 2.3 m wide, while the folded structure is 1 m wide. Figure 4.8 shows the two structures.

Here we are merely focussing on the difference as a result on the folding of the arms. In Figure 4.8 the bottom parts of the two zig-zag antennas are 1 m apart. The width of the unfolded structure is 2.3 m while the width of the folded structure is 1 m. At a half-wavelength of 2.3 m, the resonant frequency is about 65 MHz and at 1 m it is about

150 MHz. Thus by shortening the electrical length through bending the elements one expects the lower cut-off frequency to move upwards from 65 MHz to somewhere between 65 and 150 MHz. One determines this point through simulation and that is exactly what will be done next.

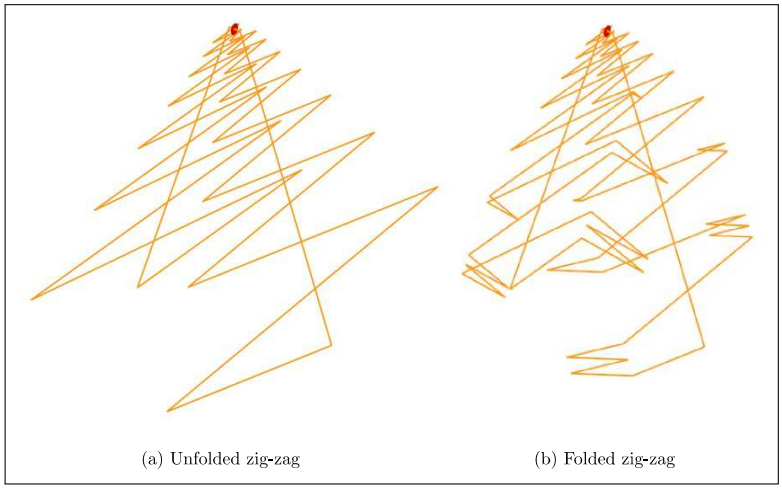

Figure 4.8: Two zig-zag antennas to be compared with each other.

The two antennas of Figure 4.8 are simulated in FEKO and the results are shown in the following figures.

Figure 4.9 shows the directivity comparison between the two configurations. Here we clearly see that the directivity only changes a little (< 1 dB) over the entire band width. Thus one can assume that the directivity remains unaltered.

Figure 4.10 shows the reflection coefficient for the two configurations. Here the reflections are exactly the same from about 200 MHz and upward. This was expected to remain the same as the longer elements do not contribute at the higher frequencies. Below this point both configurations still radiate. The folded configuration crosses the -10 dB point at 102 MHz while the unfolded configuration crosses it at 76 MHz. This means that we have lost some bandwidth unfortunately but this was expected. This shows that by reducing the structures width by more than halving it only reduces the structures bandwidth at the low frequencies by 26 MHz.

This also suggests that the following characteristics, the polarisation purity and the E- and H-plane beamwidths, we will look at next should follow a similar trend as the reflection coefficient does. One expects the high and mid frequencies to remain unaltered while the lower frequencies are expected to be different.

Figure 4.11 shows the cross- and co-polarisation as defined by Ludwig's Third Rule [22].

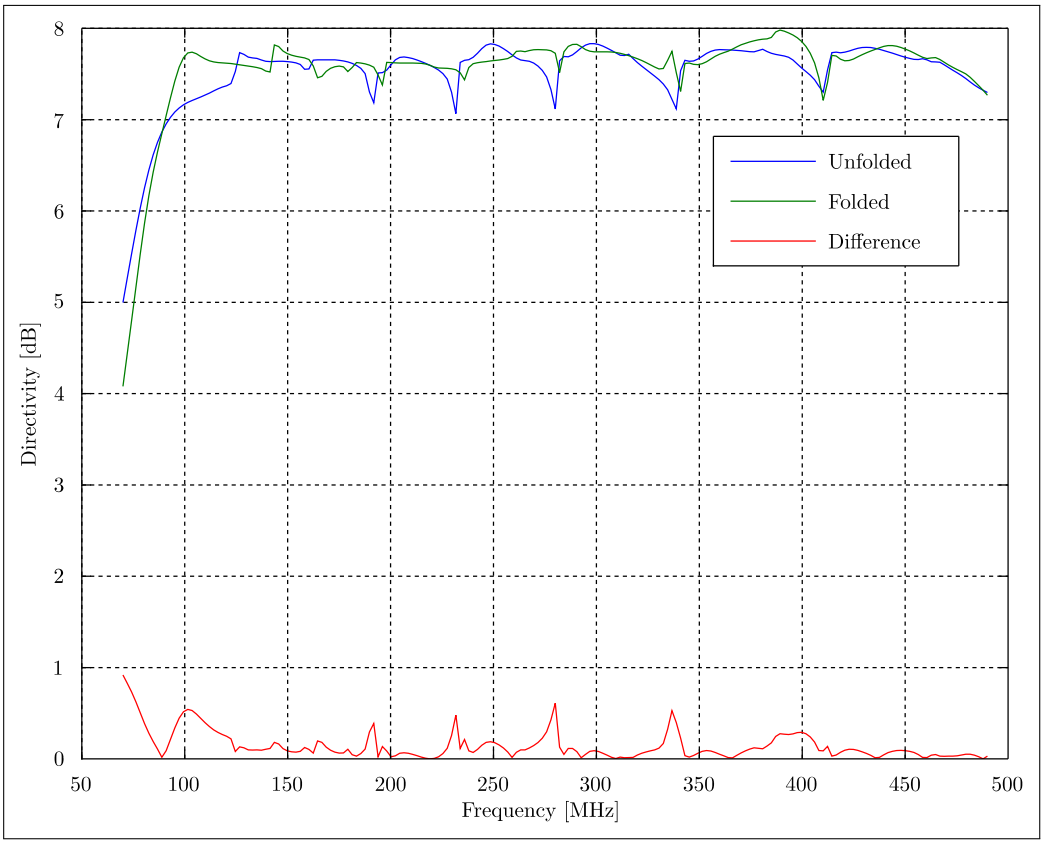

Figure 4.9: Comparison of the directivity between the folded and unfolded antenna.

Here one sees the co-polarisation is very similar to the directivity and the cross-polarisation is much less. The cross-polarisation of the two configurations is very similar over the frequency band except at the lower part. Here the folded cross-polarisation worsens quickly at about 100 MHz and downward.

Next we take a look at the E- and H-plane beamwidth. Figure 4.12 shows the beamwidth at the low frequencies. The unfolded E-plane beamwidth is 73° while folding it changes it to 81°. The unfolded H-plane is 136° while folding it changes it to 182°.

Figure 4.13 shows the beamwidth at the centre frequencies. Here one sees the E- and H-plane beamwidths are similar for the folded and unfolded cases. With the E-plane being 80° and 66° for the unfolded and folded cases respectively and the H-plane being 109° and 98° for the unfolded and folded cases respectively.

Figure 4.14 shows the beamwidth at the high frequencies. Here one sees the E- and H-plane beamwidths are identical for the folded and unfolded cases. With the E-plane being 72° for both unfolded and folded cases and the H-plane being 104° for both the unfolded and folded cases.

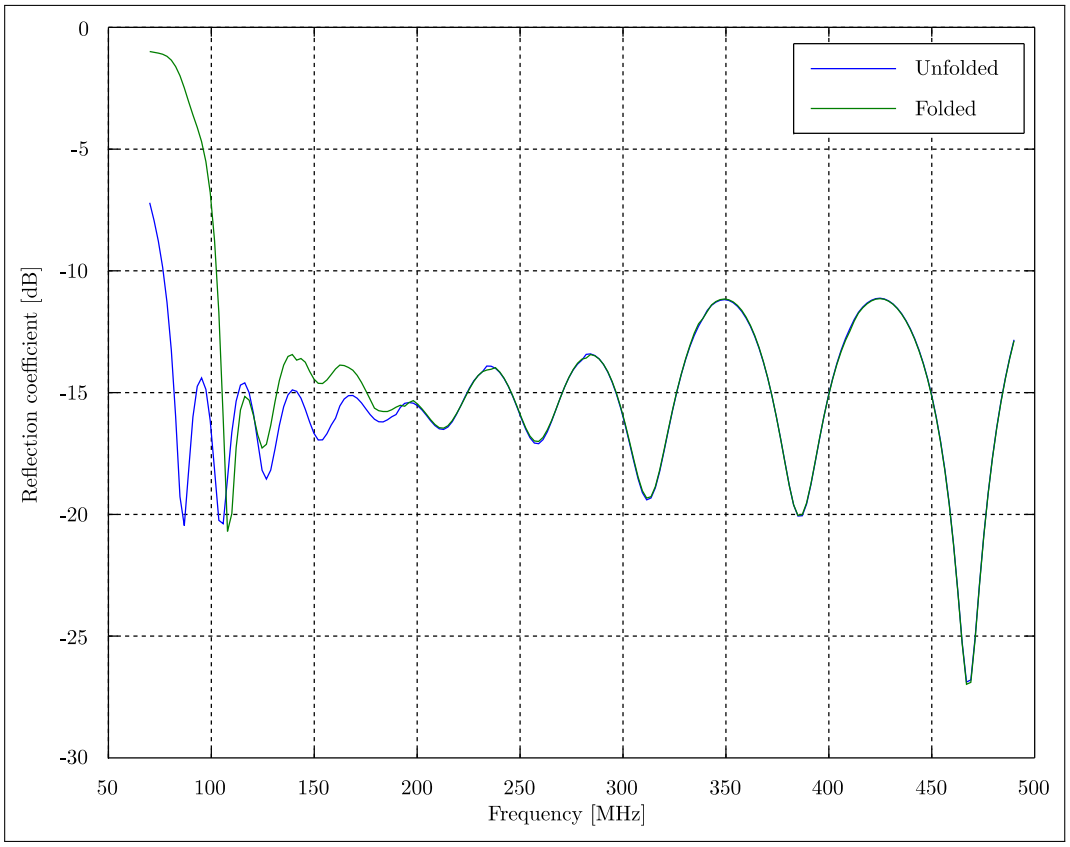

Figure 4.10: Comparison of the reflection coefficient (S_{11}) between the folded and unfolded antenna with $Z_0 = 225\Omega$.

This shows that by folding the longer elements the antenna's performance remains mostly unchanged. Only some bandwidth at the lower frequencies are lost. This is the price paid for in terms of performance for reducing the width of the antenna.

4.5 Zig-zag Feed

The antenna needs a feeding network in order to send and receive signals. A simple 50Ω cable would be ideal, but the input impedance of the antenna is about 250Ω, thus a matching network of some kind needs to be implemented.

4.5.1 Balun

The coaxial feeding cable is inherently unbalanced, while the antenna is balanced. This results in the need for a balun which can match a balanced line with an unbalanced line.

The possibility of using a differential low-noise amplifier (LNA) as a feed for the zig-zag antenna is quite attractive. A balun would no longer be needed as the balanced antenna can be directly connected to it. One drawback is it can only be used in the receive mode and not for transmitting.

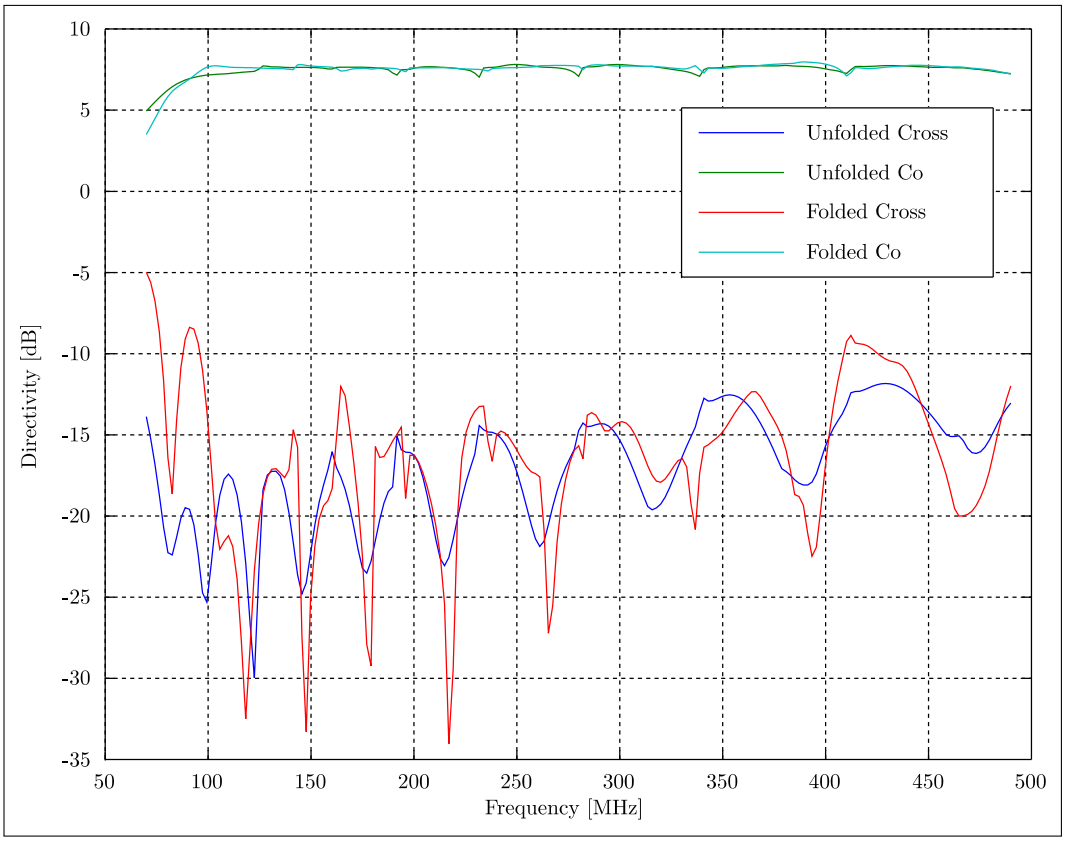

Figure 4.11: Comparison of the polarisation purity between the folded and unfolded antenna.

As the antenna has such a wide bandwidth we will need a wide band balun to go with it. Possible solutions are the Marchand balun, the infinite balun or a ferrite core transformer.

The Marchand balun works as a band-pass device with quarter-wavelength resonant transmission lines as shown by Cloete [25]. Its frequency response looks similar to a Chebyshev impedance transformer. This balun uses quarter-wavelength transmission lines and at low frequencies that this antenna is designed for would result in a physically large balun. It is usually a bit more expensive balun and contributes to the reason for not picking this balun.

The infinite balun is used usually with LPDA antennas by passing the coaxial conductor through the one arm of the antenna. The outside conductor is then connected to this arm and the inside conductor extended and connected to the other arm. This would not be possible for the zig-zag antenna we are building as we are using wires and not tubes.

The ferrite core transformer is a very good option. This transformer provides 4:1 impedance transforming and balanced and unbalanced terminals. The coaxial line conductors are wound around a ferrite core as shown in Figure 4.15. On the left side the coaxial cable is connected and on the right side the two arms of the antenna without connecting it to

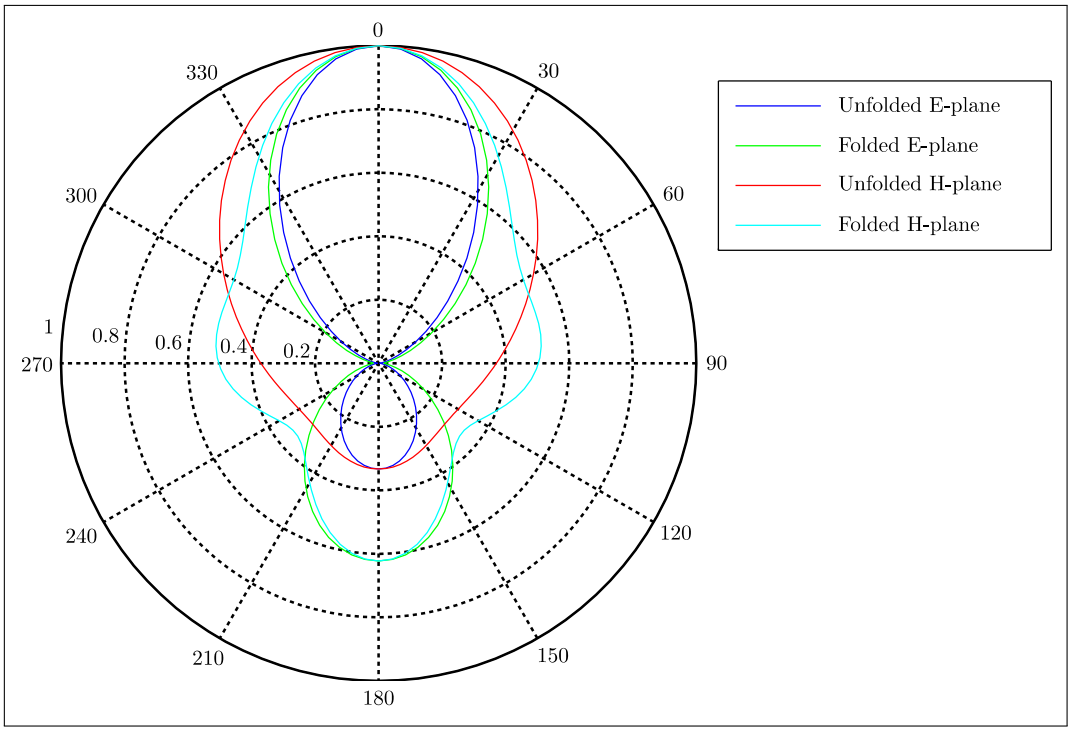

Figure 4.12: Comparison of the E- and H-plane half power beamwidth between the folded and unfolded antenna at the low frequencies.

ground. This forms a symmetrical structure and forms the balun. The ferrite core can maintain high impedance levels over a wide frequency band and with good design can provide bandwidths of up to 10:1 [1]. We choose the ferrite transformer as the balun and buy an off the shelf transformer from Mini-Circuits.

4.5.2 Physical feed measured

We chose an impedance transformer from a catalogue (Mini-Circuits) that works as the feed, one side we see 50 Ω and the other side 200 Ω thus making it a 4:1 ratio. We first build a test circuit and compare the measured results for this feed to the given results from the data sheet in Figure 4.16.

Figure 4.16 shows the reflection for this transformer from the data sheet compared to the measured result. The results are similar and thus the transformer works as intended.

4.6 Manufacturing

We used 2 mm brazing rods to build the full scale zig-zag antenna showed in Figure 4.17. We start building this antenna one zig-zag arm at a time. Figure 4.18 shows a part of one arm of the full structure. Measurements are obtained from the FEKO model and the brazing rods are cut to size. The rods/wires are soldered together to form the correct

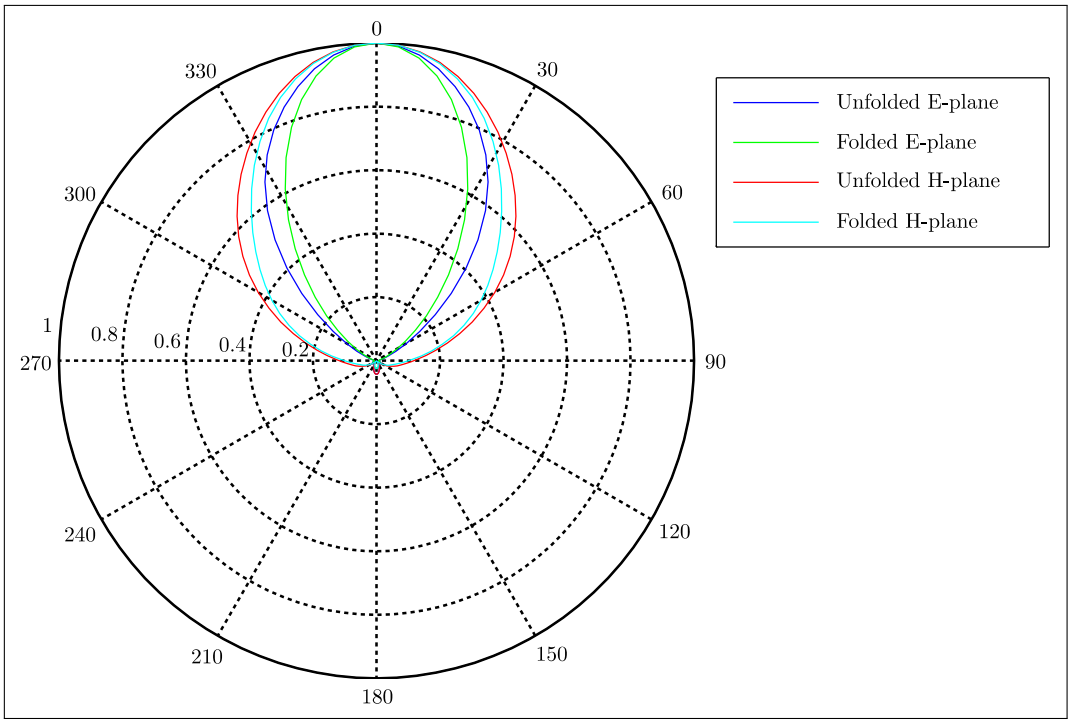

Figure 4.13: Comparison of the E- and H-plane half power beamwidth between the folded and unfolded antenna at the centre frequencies.

shape and bend where needed. The arms are stapled to the wooden frame with a staple gun in order to remain stationery. Four PVC pipes are added to the frame in order for it to stand on its side for measurements on the roof.

Seeing as the structure has a footprint of 1 m^2, it would not fit through a single door, but only double doors. This complicated matters to get the antenna on the roof without taking it apart again. It was decided to hoist the antenna up onto the roof and was done.

4.7 Antenna Measuring

Once on the roof we could start the measuring of the antenna. The reason for measuring on the roof is to negate the effect of ground reflections and to be away from interference as much as possible. The set-up is shown in Figure 4.19 with a receiving antenna on the opposite roof (not shown in figure). Before measuring we calibrated with a known antenna in order to use gain substitution for the measurements. An RFI survey was also done which showed some weak sources all around. It was decided to use maximum output power from the signal generator in order to be above the interference.

We measured the gain of the zig-zag and an E-plane pattern cut by physically rotating the antenna. All the necessary data was saved for processing later.

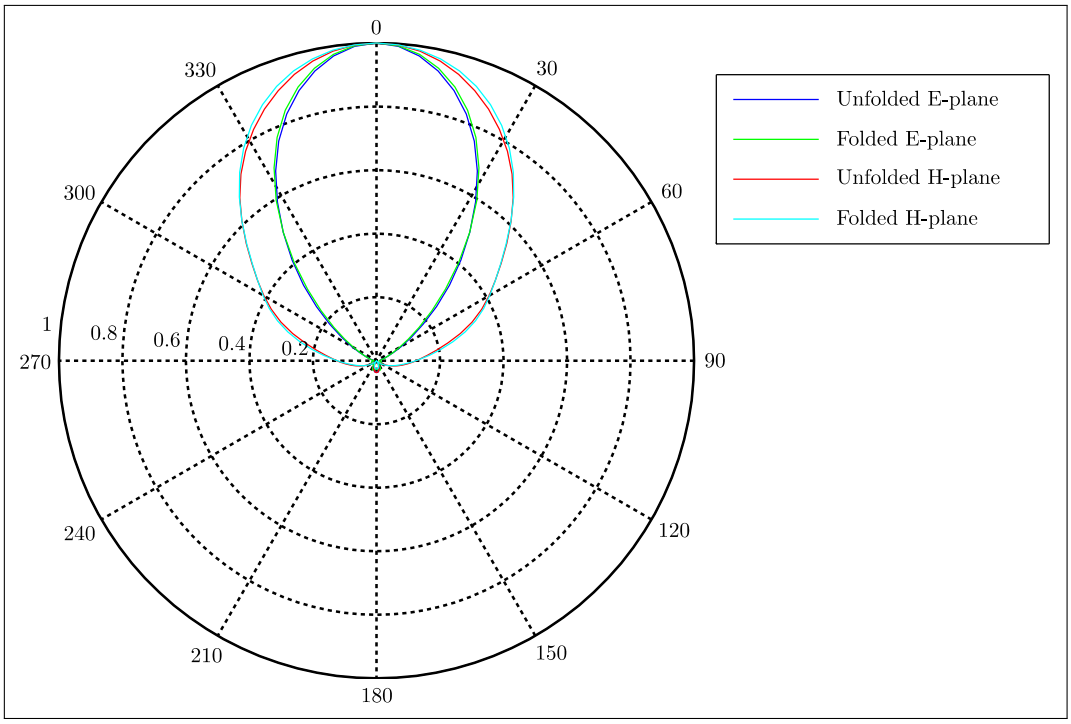

Figure 4.14: Comparison of the E- and H-plane half power beamwidth between the folded and unfolded antenna at the high frequencies.

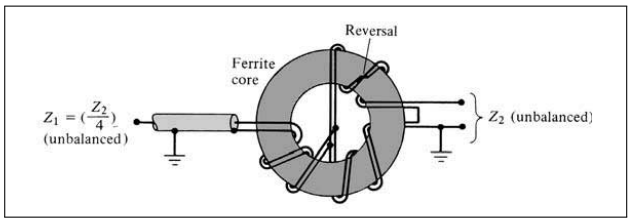

Figure 4.15: Ferrite core transformer (4:1). Source: Balanis [1].

4.8 Results

The measured data is processed and compared to the expected results from simulation. Figure 4.20 shows the measured reflection coefficient compared to the simulated reflection coefficient. The measured results are very good and stay under -10 dB the whole band.

Figure 4.21 shows the measured gain compared to the simulated gain. Here the measured results do not correlate with the simulated results due to interference. We observe asymmetries in the radiation pattern due to the surrounding environment that reflects. We would suggest repeating the measurements at an antenna test range such as Paardefontein in order to get rid of the interference.

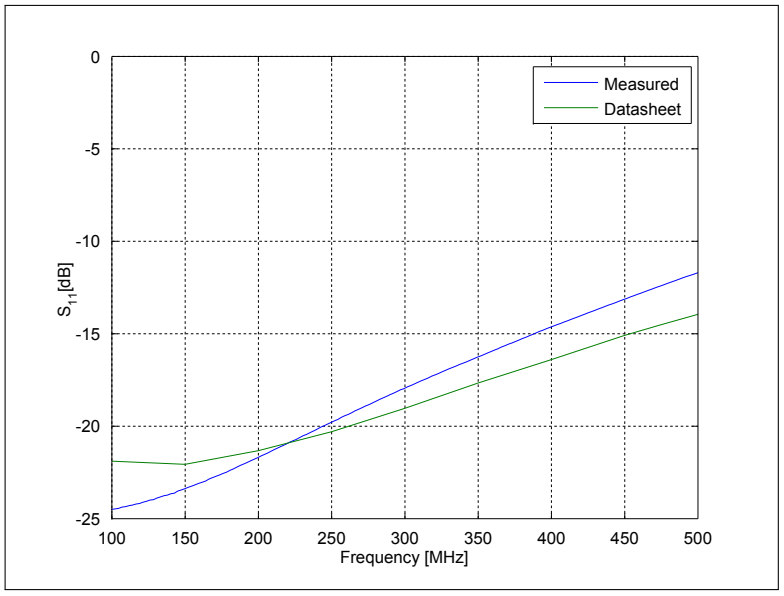

Figure 4.16: Reflection coefficient results for measured transformer compared with data sheet.

Figure 4.17: Full scale zig-zag antenna fully built and assembled.

Colleagues helped with the measurements on the day and also measured their antenna. They observed similar asymmetries to what we observed. They were fortunate enough to also test at Paardefontein in order to get rid of the interference we observed on the roof. The measured results they obtained there were much better and correlated well with the simulated results. This gives some hope for the zig-zag's unfavourable measurements as much better results could be obtained when measuring at a much better site. This

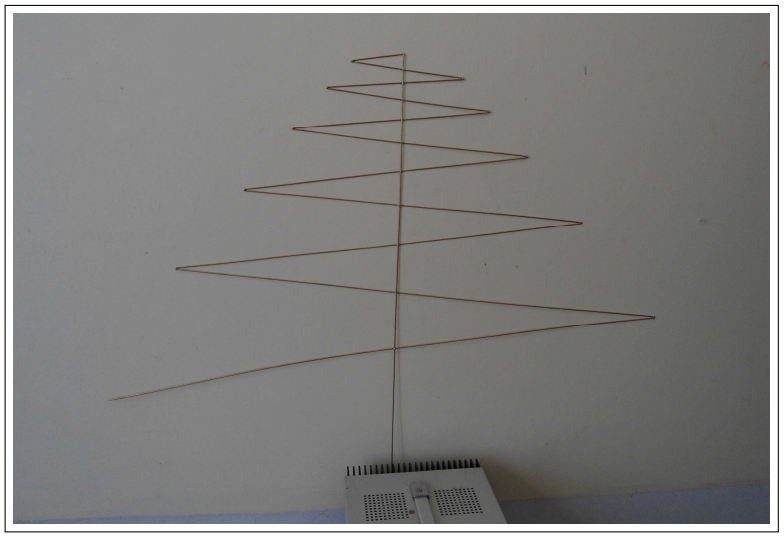

Figure 4.18: One part of the zig-zag antenna.

Figure 4.19: The measurement set-up for the zig-zag antenna.

concludes the measurements and this chapter.

4.9 Recap

In this chapter the following was discussed:

1. the design of a zig-zag antenna
2. FEKO is choice of simulation package with MoM technique
3. parameter study through simulation

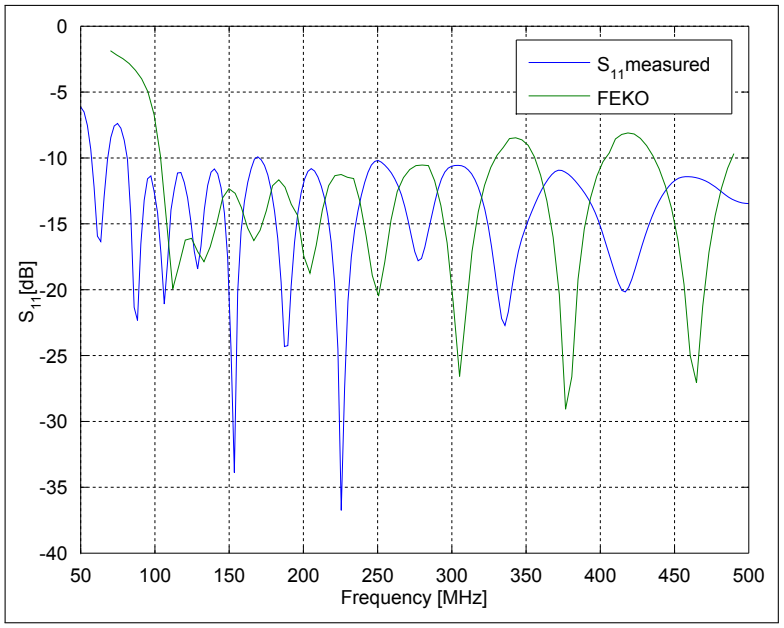

Figure 4.20: Measured reflection coefficient compared to simulated reflection coefficient.

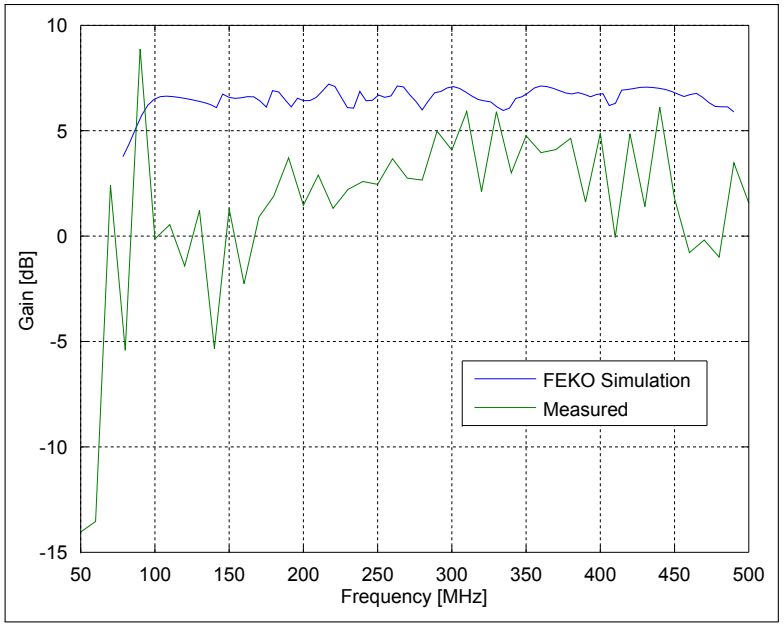

Figure 4.21: Measured gain compared to simulated gain.

4. antenna characteristics plotted (design curves) and discussed

5. manufacturing of a zig-zag antenna on wooden frame

6. measurements and discussion of measured antenna

Chapter 5

Conclusion and Recommendations

In this thesis a problem for the SKA was presented. Background for this was given and the focus was on the low frequency array of the SKA.

Two design strategies were presented, one for a printed LPDA and a second one for a zig-zag configurations. Design curves were generated for the printed LPDA and a scale model built. These measurements did not correlate with the simulation results as possible manufacturing and assembly problems interfered with the correct workings.

Design curves were also generated for the zig-zag configuration. A full scale low-cost prototype was built with low-cost brazing rods and mounted on a wooden frame. Measurements on the roof of the building were expected to be good, but in reality much interference was present. It is expected that a proper antenna test range, such as Paardefontein, would yield the expected results and correlate very closely to the simulated results.

It was shown that both of these design strategies work and would aid in designing the wanted antennas.

5.1 Future work

Possible research in the future include the cross polarisation and the feed. The cross polarisation in the zig-zag design is well above -20 dB and needs improvement. The balun that is used is very lossy, up to about 1 dB insertion loss for the transformer, and needs improvement. Other feeding methods should also be investigated.

5.2 Final Recommendation

The zig-zag design presented here could be a possible candidate for the SKA low frequency array. The balun used proved to be quite lossy and the cross polarisation is probably not good enough. The beamwidth specification of 90° was not met, but there could

be a fundamental problem here. This antenna seems very cheap to build and if mass production is sorted out this antenna would be a very good candidate.

Appendices

Appendix A

Appendix: Design example for Carrel's LPDA

An example of Carrel's design strategy will be executed when given certain specifications. This example is taken from Balanis [1] and repeated here.

A.1 Specifications

Assume the following specifications:

- Bandwidth must be 54 to 216 MHz
- Directivity of 8 dB
- 50 Ω input impedance
- Dipoles diameter's should be 1.9 cm for largest dipole and 0.48 cm for the smallest dipole

A.2 Solution

1. Using Figure 2.10 we find the optimum σ and accompanying τ values to be 0.157 and 0.865.
2. With equation 2.22 we calculate α
   $\alpha = \tan^{-1}\left[\frac{1-0.865}{4(0.157)}\right] = 12.13^\circ \approx 12^\circ$
3. Calculating B_{ar} with equation 2.23
   $B_{ar} = 1.1 + 7.7(1-0.865)^2\cot(12.13^\circ) = 1.753$
   and B_s using equation 2.24
   $B_s = BB_{ar} = \frac{216}{54}(1.753) = 4(1.753) = 7.01$

4. The maximum wavelength is calculated as
   $\lambda_{max} = \frac{v}{f_{min}} = \frac{3\times10^8}{54\times10^6} = 5.556$ m
   The total length is gained from equation 2.25 as
   $L = \frac{5.556}{4}\left(1 - \frac{1}{7.01}\right)\cot(12.13^\circ) = 5.541$ m
   and the number of dipoles from equation 2.26
   $N = 1 + \frac{\ln(7.01)}{\ln(1/0.865)} = 14.43$ (meaning 14 or 15 elements)

5. $\sigma' = \frac{\sigma}{\sqrt{\tau}} = \frac{0.157}{\sqrt{0.865}} = 0.169$
   The longest dipole is
   $l_{max} = \frac{\lambda_{max}}{2} = \frac{5.556}{2} = 2.778$ m
   $\frac{l_{max}}{d_{max}} = \frac{2.778}{0.019} = 145.816$
   and using equation 2.27gives
   $Z_a = 120[\ln(145.816) - 2.25] = 327.88\ \Omega$
   thus producing
   $\frac{Z_a}{R_{in}} = \frac{327.88}{50} = 6.558$

6. Using Figure 2.11 gives
   $Z_0 \approx 1.2R_{in} = 1.2(50) = 60\ \Omega$

7. We assume that the feeder line is made from the same diameter that the longest dipole is made from. Now using equation 2.28 it gives us the spacing of the centres between the feeder line conductors as
   $s = 19\cosh\left(\frac{60}{120}\right) = 21.4$ mm
   This spacing allows for a 2.4 mm separation between the two conductors of the feeder line.

A.3 Simulation

This design was implemented and simulated in FEKO and the results are shown in the following figures.

Figure A.1 shows the simulated directivity over the frequency band. Here one sees that the average directivity is about 8 dB as designed for with a minimum of 7 dB and a maximum of 9.5 dB. This results in a change of 2.5 dB over the band and can be reduced by increasing the number of dipoles in the array.

Figure A.2 show the simulated reflection coefficient over the frequency band. Here one observes that the reflection stays under the -10 dB line over the whole band except for one peak of -9.4 dB at 68.6 MHz. The normalised impedance here is unfortunately 100 Ω instead of the expected 60 Ω. This is mainly due to the feeding of this antenna and a possible solution is to use an impedance transformer to correct this.

This design is quite easy and good results are easily obtained.

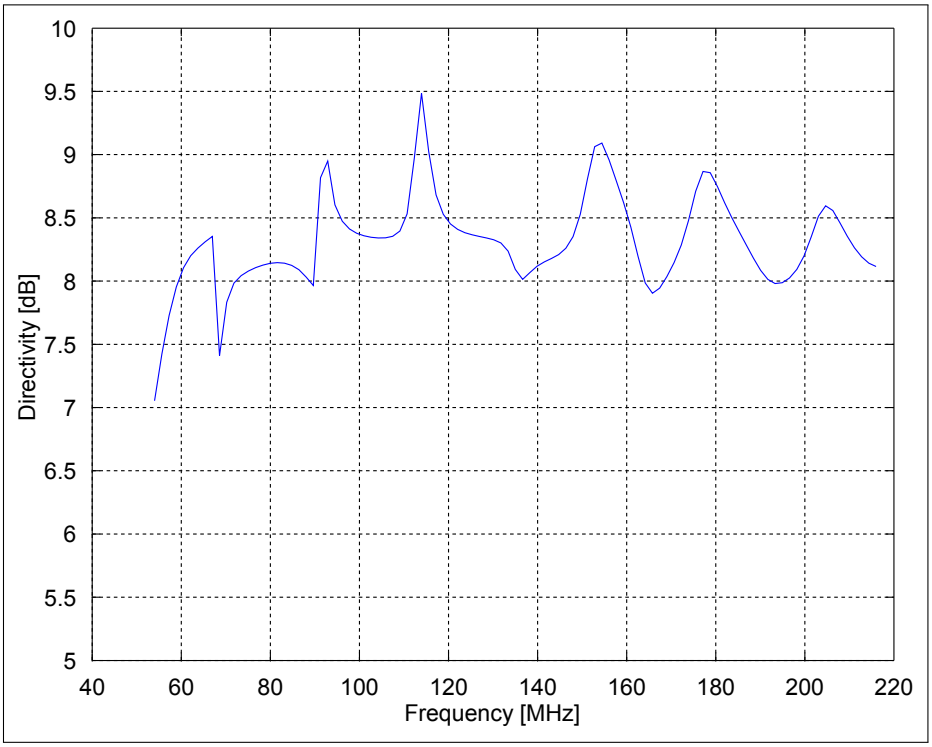

Figure A.1: Directivity for Carrel's design example

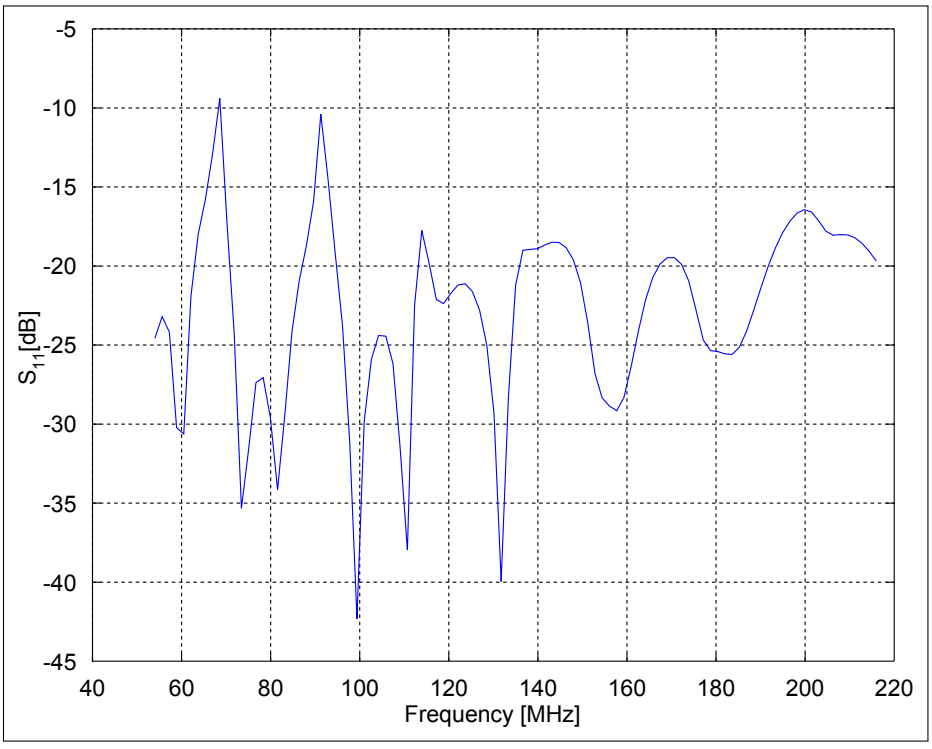

Figure A.2: S_{11} for Carrel's design example with $Z_0 = 100$

Appendix B

Appendix: Data sheet for Impedance Transformer

Surface Mount

RF Transformer

TC4-1W-17LN+

50Ω 100 to 500 MHz

CASE STYLE: AT224-1
PRICE: $1.19 ea. QTY (100)

+ RoHS compliant in accordance with EU Directive (2002/95/EC)

The +Suffix has been added in order to identify RoHS Compliance. See our web site for RoHS Compliance methodologies and qualifications.

Maximum Ratings

Operating Temperature	-40°C to 85°C
Storage Temperature	-55°C to 100°C
RF Power	0.25W
DC DWV	500V
DC Current (Primary)	0mA
DC Current (Secondary)	150mA*
Insulation Resistance Pri to Sec	1M Ohms

*Applied through center tap, equal current to secondary dot & secondary.

Permanent damage may occur if any of these limits are exceeded.

Features

- wideband, 100 to 500 MHz
- good return loss
- plastic base with leads
- aqueous washable

Applications

- push-pull amplifier
- impedance matching

Pin Connections

PRIMARY DOT	6
PRIMARY	4
SECONDARY DOT	1
SECONDARY	3
SECONDARY CT	2

Outline Drawing AT224-1

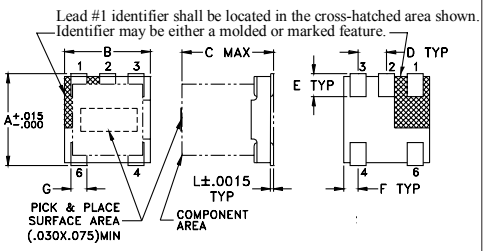

PCB Land Pattern

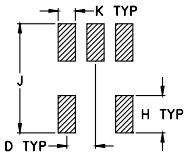

Suggested Layout,
Tolerance to be within ±.002

Outline Dimensions (inch/mm)

A	B	C	D	E	F
.150	.150	.160	.050	.040	.025
3.81	3.81	4.06	1.27	1.02	0.64

G	H	J	K	L	wt
.028	.065	.190	.030	.007	grams
0.71	1.65	4.83	0.76	0.18	0.15

Config. A

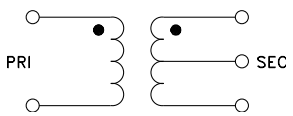

Transformer Electrical Specifications

Ω RATIO (Secondary/ Primary)	FREQUENCY (MHz)	INSERTION LOSS* 1 dB MHz	PHASE UNBALANCE (Deg.) Typ.	AMPLITUDE UNBALANCE (dB) Max.	RETURN LOSS (dB) Typ.
4	100 - 500	100 - 500	3	1.0	10

*Insertion Loss is referenced to mid-band loss, 0.6 dB typ.

Typical Performance Data

FREQUENCY (MHz)	INSERTION LOSS (dB)	INPUT R. LOSS (dB)
100.00	0.66	21.89
150.00	0.64	22.06
200.00	0.65	21.32
250.00	0.66	20.30
300.00	0.68	19.03
350.00	0.72	17.66
400.00	0.76	16.40
450.00	0.82	15.09
475.00	0.85	14.51
500.00	0.89	13.95

TC4-1W-17LN+
INSERTION LOSS

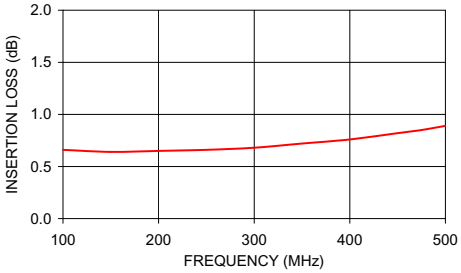

TC4-1W-17LN+
INPUT RETURN LOSS

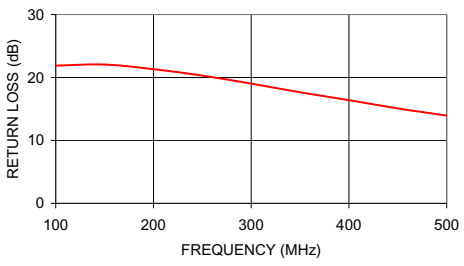

REV. A
M131604
TC4-1W-17LN+
IG/CP
110613

List of References

[1] C. Balanis, *Antenna Theory Analysis and Design*. Wiley, second edition ed., 1997. [cited at p. x, xi, 6, 7, 9, 10, 11, 15, 16, 17, 18, 19, 20, 21, 22, 23, 24, 25, 40, 65, 67, 74]

[2] R. Carrel, *Analysis and Design of the Log-Periodic Dipole Antenna*. PhD thesis, Electronic Engineering Department, University of Illinois, University Microfilms, Inc., Ann Arbor, MI, 1961. [cited at p. x, 3, 4, 20, 21, 22, 27, 33]

[3] *Antennas, Antenna Masts and Mounting Adaptors*. American Electronic Laboratories, Inc., Lansdale, PA, Catalog 7.5M-7-79. [cited at p. x, 25]

[4] F. Dubrovka, M. Lytvyn, S. Lytvyn, S. Martynyuk, Y. Ryabkin, and O. Vtorov, "Ultrawideband log-periodic dipole antenna arrays for the frequency range 0.7-12 GHz," *5th International Conference on Antenna Theory and Techniques*, pp. 110–115, May 2005. [cited at p. x, 3, 4, 32, 33]

[5] S. K. Sharma, "Investigations on miniaturized endfire vertically polarized quasi-fractal log-periodic zigzag antenna," *IEEE Transactions on Antennas and Propagation*, 2004. [cited at p. xi, 24, 60]

[6] SKA Organisation, "SKA." Available at : `http://www.skatelescope.org/`, [2012, September 7], 2012. [cited at p. 1, 2]

[7] SKA South Africa, "Square Kilometre Array (SKA) Africa." Available at : `http://www.ska.ac.za/`, [2012, September 7], 2012. [cited at p. 1, 2]

[8] A. R. Thompson, J. M. Moran, and G. W. Swenson, *Interferometry and Synthesis in Radio Astronomy*. Wiley-VCH Verlag GmbH & Co. KGaA, second edition ed., 2001. [cited at p. 1]

[9] S. Padhi, "Antenna standardization report," tech. rep., ICRAR, Australia, 2012. [cited at p. 3, 58]

[10] E. de Lera Acedo, "Antenna standardization report," tech. rep., Cambridge, UK, 2012. [cited at p. 3]

[11] G. Virone, "Antenna standardization report," tech. rep., INAF, Italy, 2012. [cited at p. 3]

[12] R. DuHamel and D. Isbell, "Broadband Logarithmically Periodic Antenna Structures," *1957 IRE National Convention Record*, vol. 1, pp. 119–128, 1957. [cited at p. 3, 10, 15, 16, 54]

[13] D. Isbell, "Log periodic dipole arrays," *IRE Transaction Antennas Propagation*, vol. AP-8, pp. 260–267, May 1960. [cited at p. 3, 17]

[14] R. DuHamel and F. Ore, "Logarithmically periodic antenna design," *IRE National Convention Record*, vol. 1, pp. 139–152, 1958. [cited at p. 4, 54]

[15] B. Guru and H. Hiziroğlu, *Electromagnetic Field Theory Fundamentals*. Cambridge University Press, second ed., 2004. [cited at p. 9]

[16] V. Rumsey, "Frequency independent antennas," *IRE National Convention Record*, vol. 1, pp. 114–118, 1957. [cited at p. 10]

[17] R. Elliott, "A view of frequency independent antennas," *The Microwave Journal*, pp. 61–68, December 1962. [cited at p. 10]

[18] J. Dyson, "The equiangular spiral antenna," *IRE Transaction Antenna Propagation*, vol. AP, pp. 181–187, April 1959. [cited at p. 13]

[19] P. Butson and G. Thompson, "A note on the calculation of the gain of log-periodic dipole antennas," *IEEE Transaction Antennas Propagation*, vol. AP, pp. 306–313, July 1976. [cited at p. 20]

[20] D. B. Davidson, *Computational Electromagnetics for RF and Microwave Engineering*. Cambridge University Press, 2005. [cited at p. 28, 29, 30]

[21] D. Pozar, *Microwave and RF Design of Wireless Systems*. John Wiley & Sons, Inc., 2001. [cited at p. 38]

[22] A. C. Ludwig, "The definition of cross polarization," *IEEE Trans. Antennas Propagat.*, vol. AP-21, pp. 116–119, Jan. 1973. [cited at p. 39, 61]

[23] R. Mattingly, P. Hannan, M. Wheeler, and et al., "IEEE standard definitions of terms for antennas," *IEEE Trans. Antennas Propagat.*, vol. AP-17, pp. 262–269, May 1969. [cited at p. 39]

[24] A. Djordjevič, R. Biljič, V. Likar-Smiljanič, and T. Sarkar, "Wideband frequency-domain characterization of FR-4 and time-domain causality," *IEEE Transactions on Electromagnetic Compatibility*, vol. 43, pp. 662–667, November 2001. [cited at p. 50]

[25] J. Cloete, "Exact design of the marchand balun," *Microwave Journal*, vol. 23, no. 5, pp. 99–102, 1980. Reprinted in J.L.B. Walker et.al. [cited at p. 64]